THE UNIVERSITY OF MANITOBA

GEOCHEMISTRY OF THE AULNEAU GRANITIC BATHOLITH, DISTRICT OF KENORA, ONTARIO, CANADA

by

MICHAEL EARL CHUTE

A THESIS SUBMITTED TO THE FACULTY OF GRADUATE STUDIES IN PARTIAL FULFILLMENT OF THE REQUIREMENTS FOR THE DEGREE OF MASTER OF SCIENCE

DEPARTMENT OF EARTH SCIENCES

WINNIPEG, MANITOBA

February, 1977

"GEOCHEMISTRY OF THE AULNEAU GRANITIC BATHOLITH,

DISTRICT OF KENORA, ONTARIO, CANADA"

by

MICHAEL EARL CHUTE

A dissertation submitted to the Faculty of Graduate Studies of the University of Manitoba in partial fulfillment of the requirements of the degree of

MASTER OF SCIENCE

TABLE OF CONTENTS

LIST OF FIGURES

LIST OF TABLES

LIST OF APPENDICES

ABSTRACT

The Aulneau batholith is an Early Precambrian, composite, granitic pluton which is exposed over an area of 1100 square kilometers in the Lake of the Woods area of northwestern Ontario. The batholith intrudes east trending Keewatin metavolcanic and metasedimentary rocks of the Kenora block of the Superior Province. Nineteen major intrusive phases that range from gabbro to quartz monzonite have been identified; the average composition of the batholith is that of a granodiorite.

The geochemistry of the batholith is based on 43 whole rock major and trace element analyses. Major elements determined include SiO_2, Al_2O_3, Fe_2O_3, FeO, CaO, MgO, Na_2O, K_2O, TiO_2, P_2O_5, MnO, H_2O, S and CO_2. Trace elements determined include Li, Pb, Ni, Cu, Co, Zn, Rb, Sn and Cs.

The batholith is characterized by a relatively constant FeO/MgO ratio with respect to increasing total alkalies and increasing SiO_2, low total alkalies, and an increasing K_2O/Na_2O ratio with respect to increasing SiO_2 content. These characteristics indicate the calc-alkaline nature of the batholith.

The trace element behaviour within the batholith is generally consistent with the behaviour of the major elements with which the trace elements are associated. Li, Co, Ni, Cu and Zn decrease in concentration with increasing differentiation. Pb and Rb increase

in concentration with increasing differentiation.

The origin of the Aulneau batholith magmas, when considered in the light of theories for the origin of calc-alkaline igneous rock suites, are best explained by the partial melting of quartz eclogite under wet conditions ($P_{H_2O} < P_{Load}$) at 27 to 36 kilobars. The major evidence in support of this interpretation are the low K_2O/Na_2O ratios observed in the Aulneau batholith.

INTRODUCTION

Statement of the Problem

Geologic mapping by geologists of the Centre for Precambrian Studies, University of Manitoba, has shown that the Aulneau batholith is a complex composite granitic intrusion composed of at least nineteen major phases ranging in composition from gabbro to quartz monzonite.

Geochemical investigations of the Early Precambrian rocks of the western part of the Superior Province of the Canadian Shield have focused mainly on the metavolcanic rocks of the "greenstone belts" to the partial exclusion of the granitic batholiths which intrude them.

The object of this preliminary geochemical investigation is to document the major and trace element composition of the batholith and to interpret the compositional variations with respect to possible mechanisms of origin of the batholith.

Area of Investigation

The area of investigation in which the Aulneau granitic batholith rests includes the Aulneau Peninsula in the Lake of the Woods, District of Kenora, Ontario. The batholith underlies 1,100 square kilometers of the peninsula and surrounding islands, and is located between $49^{o}11'$ and $49^{o}29'$ north latitude, and $94^{o}02'$ and $94^{o}43'$ west longitude (Figure 1).

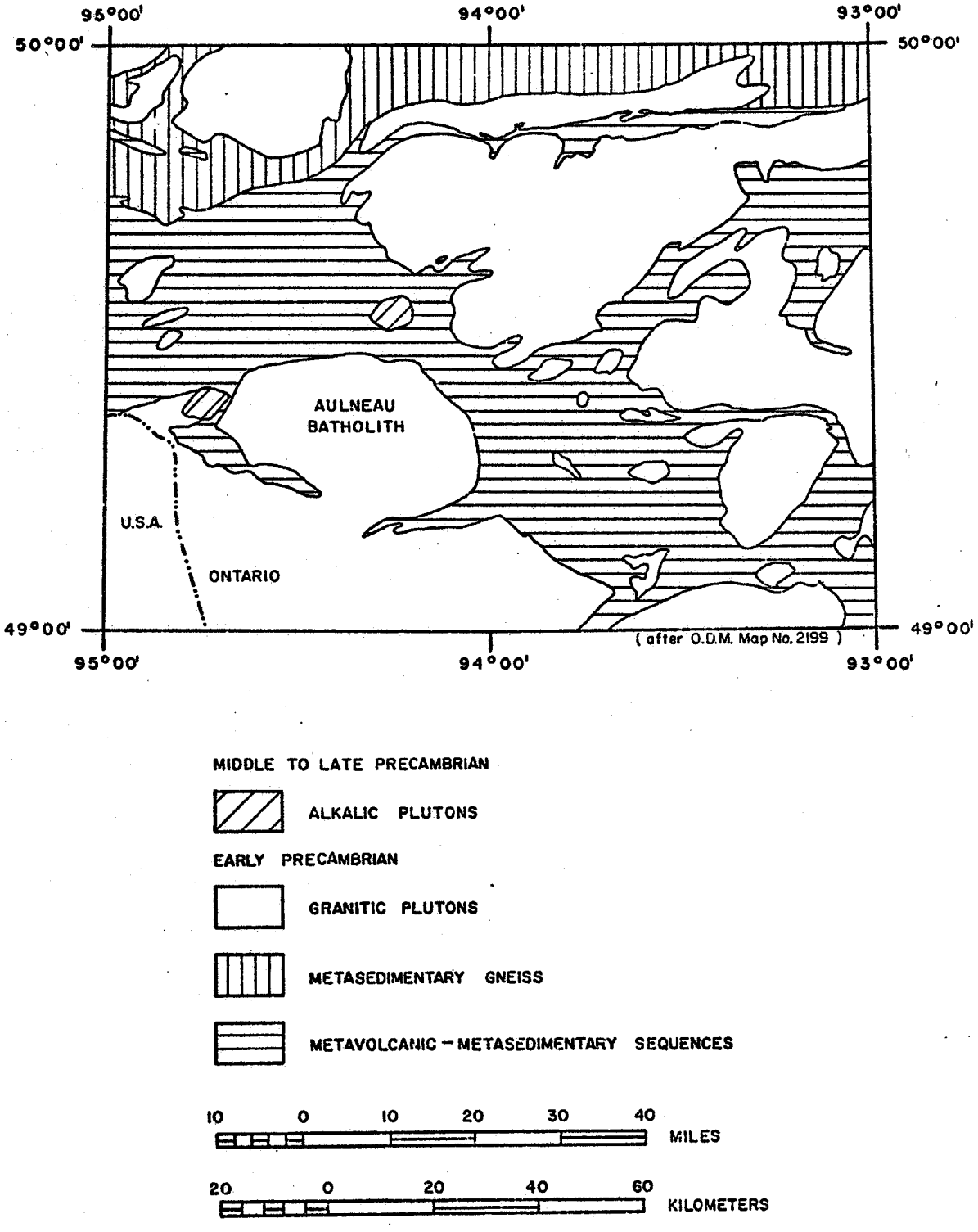

Figure 1. Index map and regional geology of the Lake of the Woods area.

Previous Geological Work

The first detailed geological investigations of the Lake of the Woods area were made by A.C. Lawson between 1883 and 1885 (Lawson, 1885). He observed that the line of contact between the hornblende-schists and the granitoid gneiss was that of an extensive ellipse which outlined the Aulneau Peninsula which was then known as Grande Presqu'isle. Lawson states that:

> "... This encircling zone of schists embraces within it a great central area of coarse, granitoid gneiss, well displayed on the shores and islands of Whitefish Bay, on the shores of the Grande Presqu'isle, and on the inlets and lakes which extend into its' interior. The whole structure is that of an immense anticlinal dome of upheaved gneiss, upon which are arranged, concentrically to its' outlines, the hornblende-schists of the higher series."

Lawson made no attempt to subdivide the granitoid gneiss of Grande Presqu'isle.

The northwestern edge of the Aulneau Peninsula was described by J.E. Thomson (Thomson, 1936). He recognized that variations in composition, structure and texture occurred within the granitoid rocks but made no attempt to map out the intrusive phases.

N.H.C. Fraser mapped the Whitefish Bay area of Lake of the Woods in 1937 (Fraser, 1943). Fraser recognized that the Aulneau Peninsula was comprised of granite and porphyritic granite but made no attempt to outline the different phases.

The first detailed geological investigations of the Aulneau batholith were conducted by D.V. Ziehlke of the Centre for Precambrian Studies, University of Manitoba, during the 1972, 1973 and 1974 field seasons. Nineteen intrusive phases ranging in composition from gabbro to quartz monzonite have been identified (Ziehlke, 1974).

Method of Investigation

This study of the Aulneau batholith is a reconnaissance geochemical investigation based on forty-three whole rock major and trace element chemical analyses. The samples were collected by Mr. D.V. Ziehlke during field mapping in the 1972 and 1973 field seasons. The samples were selected for chemical analysis by Mr. Ziehlke on the basis that they were thought to be representative of the phases as identified by field criteria. Reclassification of the analysed samples, based on laboratory investigations by the Centre for Precambrian Studies, resulted in an unequal distribution of samples with regard to the number of samples in each intrusive phase. The sample population is comprised of 7 early intrusive phase samples, 15 middle intrusive phase samples and 21 late intrusive phase samples.

Approximately one kilogram of each sample was crushed during sample preparation to minimize the effect of large phenocrysts and porphyritic textures. The samples were analysed by Mr. K. Ramlal and Mr. R. Chapman of the Department of Earth Sciences, University of Manitoba. SiO_2, Al_2O_3, total iron as FeO, MgO, CaO, K_2O, TiO_2 and MnO were determined by X-ray fluorescence spectrometry. Na_2O, low MgO, Li, Pb, Ni, Cu, Co, Zn, Rb, Sn and Cs were determined by atomic absorption spectrophotometry. FeO and S were determined by titration, P_2O_5 was determined colorimetrically, and H_2O and CO_2 were determined by loss on ignition. The analytical methods, precision and accuracy are summarized in Appendix 1. The chemical analyses are listed in Appendix 2.

Slabbed and stained hand specimens of the samples selected for chemical analysis were point counted for quartz, plagioclase,

potassium feldspar, and mafic and accessory minerals. Thin sections were point counted to determine the relative abundances of the mafic and accessory minerals. The thin sections were also examined to determine textural and structural characteristics of the samples, the type and degree of alteration, and plagioclase composition. The modal mineralogy of the samples is tabulated in Appendix 3. Twenty of the modal analyses based on slabbed and stained hand specimens were supplied by the Centre for Precambrian Studies.

The chemical data was analysed to determine geochemical trends and interelement relationships. C.I.P.W. normative mineralogies were calculated to facilitate comparison with published data. The C.I.P.W. normative mineralogy of the thesis samples is tabulated in Appendix 4.

Acknowledgements

The author gratefully acknowledges Drs. H.D.B. Wilson, W.C. Brisbin and L.D. Ayres of the University of Manitoba for their guidance and assistance, and Dr. R.F.J. Scoates of the Manitoba Department of Mines, Resources and Environmental Management for critical examination of the manuscript.

The study was supported financially by the Department of Earth Sciences, University of Manitoba, and Dr. H.D.B. Wilson through a National Research Council Grant.

The author wishes to acknowledge Mr. D.V. Ziehlke of the Centre for Precambrian Studies for the geological base map, samples used in the study and the slabbed and stained modal analyses for twenty samples. Likewise, the author wishes to acknowledge Mr. H. Ambach for assistance with computer programs and Dr. A. Green for the Kolmogorov-Smirnov analysis of the elemental distributions.

GEOLOGY OF THE AULNEAU BATHOLITH

Regional Setting

The Aulneau batholith is an Early Precambrian, oval-shaped, granitic intrusion which underlies 1,100 square kilometers of the Kenora block of the Superior Province in the Lake of the Woods area (Figure 1). The major axis of the batholith is 48 kilometers long and trends northwesterly, the minor axis of the batholith is 30 kilometers in length and trends southwesterly. The batholith intrudes isoclinally folded, steeply dipping Keewatin Group mafic to intermediate metavolcanic rocks and minor interbedded metasedimentary rocks. The general geology of the Keewatin Group in the Lake of the Woods - Manitou Lake - Wabigoon region of the Kenora block was described by Goodwin (1965). The crustal structure and Early Precambrian geology in the Lake of the Woods area was summarized by Wilson et. al. (1972). Hall et. al. (1974) established that the Aulneau batholith has a thickness of 16 kilometers ± 2 kilometers to the Riel 1 discontinuity. This thickness correlates with a 16 kilometer compensation level indicated by gravity studies (Brisbin, 1974).

Geology of the Batholith

The geology of the Aulneau batholith was described by Ziehlke (1972, 1973, 1974) and is shown in Figure 2. The batholith is composed of nineteen major intrusive phases and several minor aplitic and pegmatitic phases. The phases range from gabbro to quartz monzonite

in composition. The phases were identified by Ziehlke on the basis of mineralogical composition, grain size, color, texture, structure and field relationships. For a description of the intrusive phases the reader is referred to Zieklke (1974).

Ziehlke (1974) divided the phases of the Aulneau batholith into early migmatitic phases, intermediate intrusive phases and late intrusive phases. In this study the terms early intrusive phases, middle intrusive phases and late intrusive phases have been adopted to remove structural and compositional connotations. Intrusive relationships and distribution of the individual phases are summarized in Appendix 5.

The early intrusive phases include Ziehlkes' (1974) phases 1, 2 and 4. Phase 1 is subdivided into subphases 1a - 1g. Phases 1a and 1d are intrusive biotite trondhjemite complexes and hornblende - biotite trondhjemite complexes respectively that are characterized by a high degree of inhomogeneity. Phases 1b, 1c, 1e and 1g are biotite trondhjemites, phase 1f is a hornblende - biotite trondhjemite phase. Phase 2 is a biotite trondhjemite. Phase 4 is subdivided into phases 4a - 4g which range from gabbro to diorite in composition. The middle intrusive phases includes phases 3, 5, 6, 7, 8, 9, 10, 11, 12, 13 and 14. Phases 3, 5, 9, 10, 11, 12, 13 and 14 are biotite trondhmenites and granodiorites, phases 6, 7 and 8 are hornblende - biotite trondhjemites. The late intrusive phases include phases 15, 16, 17, 18a, 18b and 19. Phases 15 and 16 are biotite trondhjemites and granodiorites, phases 17 and 19 are biotite granodiorites, phase 18a ranges in composition from granodiorite to quartz monzonite and phase 18b are diorites.

The batholith intruded mafic metavolcanic rocks except in the Miles Bay area where it is in contact with plutonic rocks of the Painted Rock Island pluton (Figure 2). The contact between the metavolcanic country rocks and the batholith is generally sharp, although west of the Miles Bay area the contact is gradational over several hundred meters of injected gneiss. A zone of hornblende hornfels facies contact metamorphism up to several hundred meters wide is developed in the metavolcanic rocks adjacent to the batholith. Foliation in the metavolcanic rocks adjacent to the batholith is generally steeply dipping away from the batholith. Foliation within the granitic rocks adjacent to the metavolcanic rocks is generally parallel to the contact between the batholith and the metavolcanic rocks. Within the batholith a complex foliation pattern, apparently related to emplacement, is developed.

PETROGRAPHY

Descriptions of the rocks of the early, middle and late intrusive phases of the Aulneau batholith are presented to illustrate the general petrographic character of the batholith, and to provide a basis for comparison with other granitic batholiths.

Early Intrusive Phases

Rocks of the early intrusive phase are weakly foliated, leucocratic and medium grained, and possess a hypidiomorphic-granular texture. The samples are trondhjemites in composition (Figure 3) and contain 23.0 to 32.2 percent quartz, 55.4 to 63.5 percent plagioclase, 0.0 to 6.3 percent potassium feldspar and 2.9 to 17.2 percent combined mafic and accessory minerals.

Quartz occurs as anhedral crystals ranging in grain size from approximately 1.0 to 1.7 mm, minor amounts of quartz occur as finer grained interstitial material. Quartz crystals are generally free of inclusions and exhibit a slightly undulose extinction.

Plagioclase (An_{15}-An_{26}) occurs as medium grained (1.4 mm-2.5mm), equant to subsequant subhedral crystals. Some interstitial grains occur as small as 0.3 mm and some phenocrysts occur up to 7.0 mm in size. Plagioclase crystals are generally cloudy and weakly to moderately saussuritized. Zoned plagioclase crystals show preferrentially altered cores. Identified deuteric alteration products include very fine grained sericite, epidote and calcite.

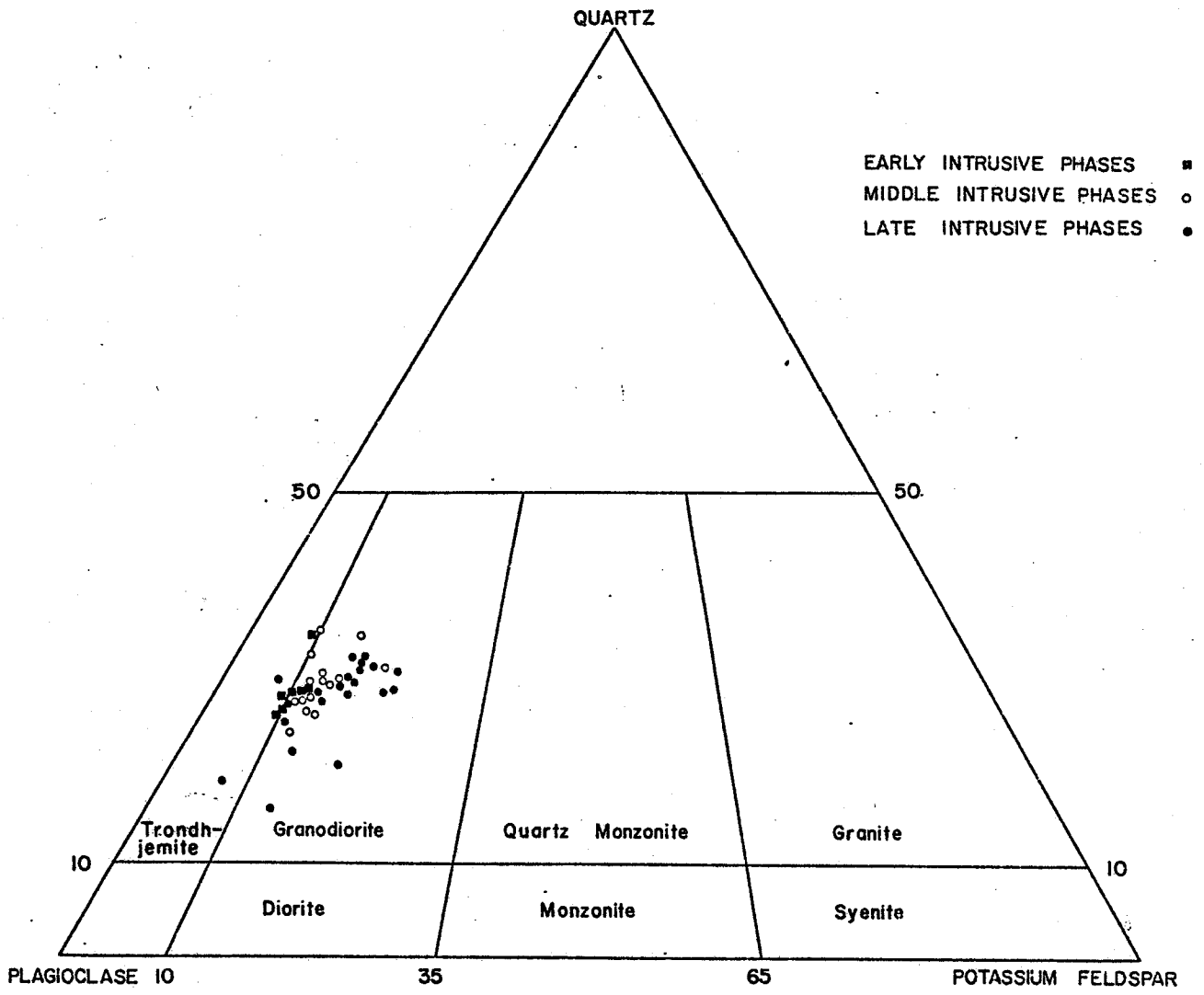

Figure 3. Modal quartz-plagioclase-potassium feldspar ternary diagram.

Potassium feldspar occurs as interstitial anhedral grains up to 0.4 mm.

Biotite, the main mafic accessory mineral, ranges from 1.9 to 9.3 percent and occurs as fine to medium grained, light brown to olive green laths. Approximately 2.0 percent of the biotite is altered to chlorite.

Hornblende comprises up to 5.9 percent of the rocks and occurs in less than half of the samples. The hornblende is generally light to dark green and occurs as medium grained euhedral to subhedral crystals.

Epidote occurs as medium sized, euhedral to subhedral crystals associated with aggregates of biotite laths. Fine grained epidote occurs as a deuteric alteration product of plagioclase. Epidote comprises 0.5 to 1.8 percent of the samples.

Sphene and iron-titanium oxides occur as fine to medium grained, euhedral to subhedral crystals which comprise 0.0 to 0.7 percent and 0.1 to 0.5 percent of the samples respectively.

Allanite, apatite and zircon occur in trace amounts which range from 0.0 to 0.1 percent. Allanite is generally surrounded by a corona of epidote. Apatite and zircon are generally found as very fine grained euhedral crystals in the biotite laths.

Middle Intrusive Phases

Rocks of the middle intrusive phase are trondhjemites and granodiorites in composition (Figure 3) and contain 18.2 to 32.7 percent quartz, 48.4 to 66.7 percent plagioclase, 1.5 to 13.7 percent potassium feldspar and 3.9 to 25.7 percent combined mafic and

accessory minerals. The samples are leucocratic and medium grained with a hypidiomorphic-granular texture. The samples exhibit a weak to moderate foliation. Hematite staining imparts a pinkish cast to some of the samples.

The majority of the quartz occurs as anhedral phenocrysts which range from 1.5 to 2.0 mm, minor amounts of quartz occurs as very fine interstitial material. The quartz is weakly to moderately undulose and generally free of inclusions.

Plagioclase phenocrysts (An_{13}-An_{26}) occur as equant to subequant, subhedral crystals which range in size from 1.5 to 3.0 mm. Compositionally zoned plagioclase phenocrysts show weak to moderate selective deuteric alteration of the more calcic plagioclase cores. Alteration products include very fine grained laths of sericite and fine grained epidote.

Potassium feldspar generally occurs as anhedral interstitial crystals ranging in size from 0.3 to 1.0 mm, however subhedral crystals ranging from 1.0 to 2.0 mm occur in some samples.

Light brown to olive green biotite comprises 0.8 to 14.3 percent of the samples and occurs as fine to medium grained subhedral laths and aggregates of laths. In the majority of the samples biotite is not altered, in the altered samples less than 10 percent of the biotite has been chloritized.

Hornblende occurs in a few samples and can constitute up to 1.3 percent of the sample. Hornblende varies from dark green to bluish green and occurs as fine to medium grained, ragged, anhedral to subhedral plates. Minor amounts of hornblende are altered to biotite.

Fine to medium grained epidote comprises 0.9 to 7.0 percent of the samples and occurs as euhedral to subhedral, sponge-like crystals.

Sphene and iron-titanium oxides occur as fine to medium grained, euhedral to subhedral crystals which comprise 0.1 to 1.8 and 0.1 to 1.1 percent of the samples respectively.

Fine grained, euhedral to subhedral apatite and zircon occur in trace amounts. Allanite occurs as fine grained, euhedral to subhedral crystals which comprise up to 0.3 percent of the samples.

Late Intrusive Phases

Rocks of the late intrusive phase are granodiorites (Figure 3) with the exception of two trondhjemites which have textural characteristics and compositions similar to the trondhjemites of the early intrusive phases. The granodiorites occur as hypidiomorphic-granular and porphyritic varieties. The hypidiomorphic-granular granodiorites are leucocratic, generally medium grained and have a weak to moderate foliation. The porphyritic granodiorites are generally massive, leucocratic and medium to coarse grained. The granodiorites contain 13.7 to 31.7 percent quartz, 42.4 to 63.2 percent plagioclase, 7.1 to 22.1 percent potassium feldspar and 4.3 to 20.3 percent combined mafic and accessory minerals.

Quartz occurs as anhedral interstitial crystals in the hypidiomorphic-granular and porphyritic granodiorites. The quartz is generally free of inclusions and has a weak to moderate undulose extinction. In the hypidiomorphic-granular granodiorites quartz ranges from approximately 0.5 mm to 2.3 mm, in the porphyritic variety the quartz ranges from 1.3 to 3.3 mm in grain size.

Plagioclase occurs as anhedral to subhedral phenocrysts in the hypidiomorphic-granular and porphyritic granodiorites. Plagioclase phenocrysts range from 1.3 to 2.9 mm in the hypidiomorphic-granular granodiorites and from 1.7 to 9.0 mm in the porphyritic granodiorites. Plagioclase compositions range from An 12 to An 20 in the hypidiomorphic-granular granodiorites and from An 8 to An 19 in the porphyritic granodiorites. In both varieties of granodiorite the plagioclase phenocrysts are zoned. Selectively altered zones suggest that the zoning is oscillatory. The degree of alteration ranges from weak to moderate with the development of very fine laths of sericite and fine grained epidote.

Potassium feldspar occurs as anhedral interstitial crystals in the hypidiomorphic-granular granodiorites and as subhedral poikilitic phenocrysts in the porphyritic granodiorites. In the hypidiomorphic-granular granodiorites the potassium feldspar ranges from 0.5 to 2.2 mm, in the porphyritic granodiorites the phenocrysts range from 1.9 to 15.0 mm. The poikilitic potassium feldspar phenocrysts enclose subhedral phenocrysts of plagioclase. String perthite is common in the potassium feldspar phenocrysts.

Biotite is the main mafic mineral in the late intrusive phases and ranges from 2.8 to 6.7 percent. It occurs as interstitial laths and aggregates of interstitial laths associated with epidote. Individual biotite laths are generally less than 1.0 mm in length. Minor amounts of biotite are altered to chlorite.

Hornblende occurs in five of the twenty-one late intrusive phase samples, in which it varies from 0.2 to 8.0 percent. The hornblende generally occurs in the porphyritic granodiorites with

the well developed potassium feldspar phenocrysts. The light brown to bluish green hornblende crystals occur as fine grained subhedral plates and as fine to medium grained aggregates of subhedral plates. Minor amounts of hornblende are altered to biotite.

Epidote generally occurs as sponge-like, fine to medium grained, subhedral crystals associated with aggregates of biotite and/or hornblende. Epidote also occurs as a fine grained alteration product of plagioclase. Epidote comprises from 0.7 to 3.7 percent of the samples.

Sphene and iron-titanium oxides compose from 0.0 to 1.9 and 0.1 to 1.2 percent of the samples respectively, both minerals occur as fine to medium grained, euhedral to subhedral crystals.

Allanite, apatite and zircon occur as fine grained, euhedral to subhedral crystals. The minerals are present in trace amounts up to a maximum of 0.3, 0.2 and 0.1 percent respectively.

Mineralogical Variation

The relationships among the major mineralogical components of the Aulneau batholith samples are shown in Figure 3, the modal quartz-plagioclase-potassium feldspar ternary diagram and Figure 4, the modal quartz-feldspar-mafic ternary diagram. Figure 3 illustrates that the compositional fields of the early, middle and late intrusive phases overlap, and that the compositional field taken as a whole represents a normal differentiation trend of increasing potassium feldspar/plagioclase ratio at a relatively constant quartz/ total feldspar ratio. Taken independently, the trend of the quartz/ potassium feldspar ratio decreases from approximately 3:1 in the

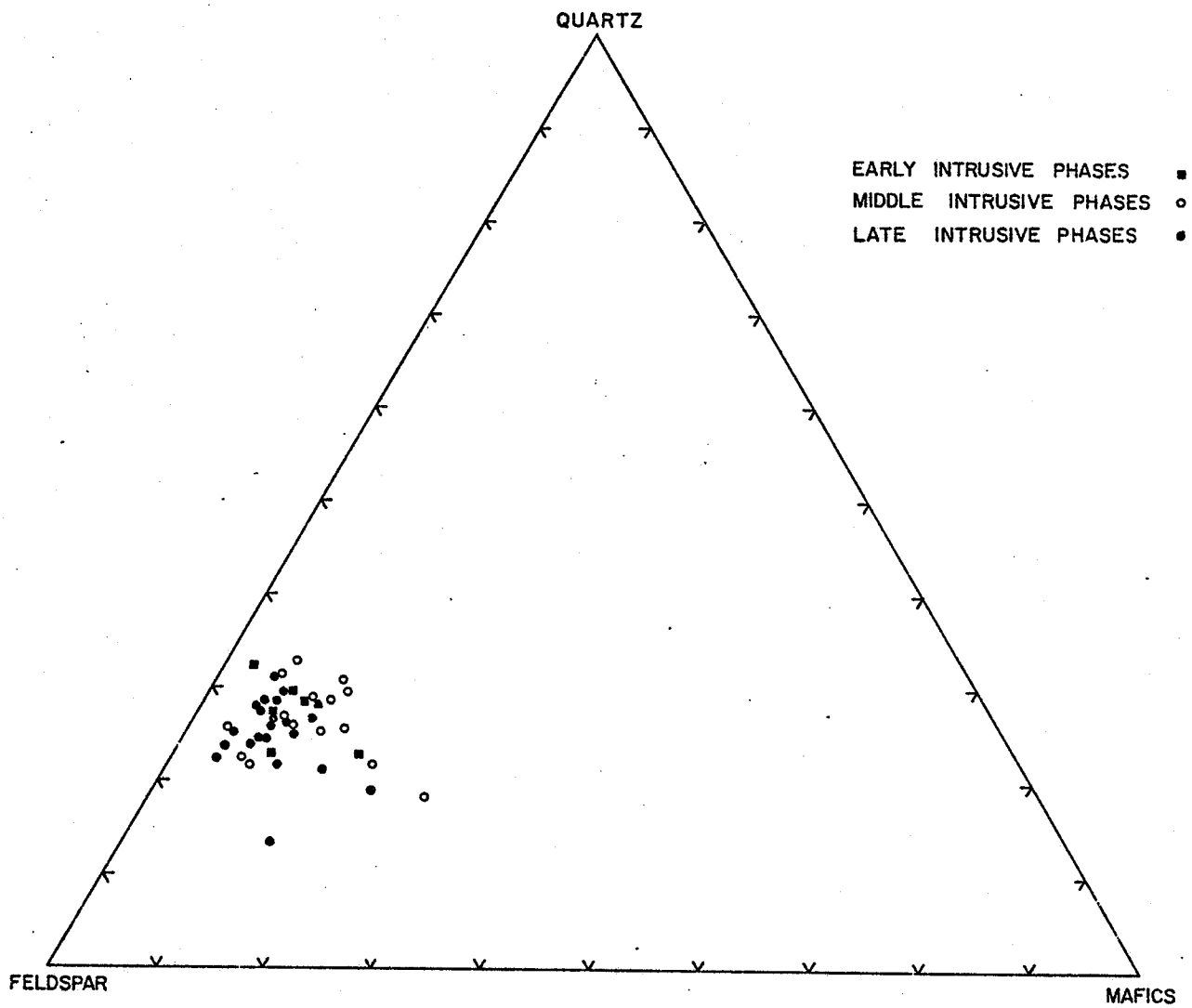

Figure 4. Modal quartz-feldspar-mafic mineral ternary diagram.

early intrusive phases to 1:1 in the middle intrusive phases and to 1:2 in the late intrusive phases. Figure 4 illustrates that the compositional fields of the early, middle and late intrusive phases overlap in a restricted field. No diagnostic trends can be identified in Figure 4.

Figure 5, the normative quartz-plagioclase-potassium feldspar ternary diagram illustrates that the range in normative compositions is limited and is characterized by a trend of increasing quartz and potassium feldspar between the early, middle and late intrusive phases. Figure 6, the normative quartz-plagioclase-potassium feldspar ternary diagram illustrates the comparison between the Aulneau batholith and other granitic bodies. The average normative mineral trend of the Aulneau batholith is not identical to any particular batholith but it is generally similar to the trend of the Southern California batholith, the Bald Mountain batholith and the Mount Garibaldi area.

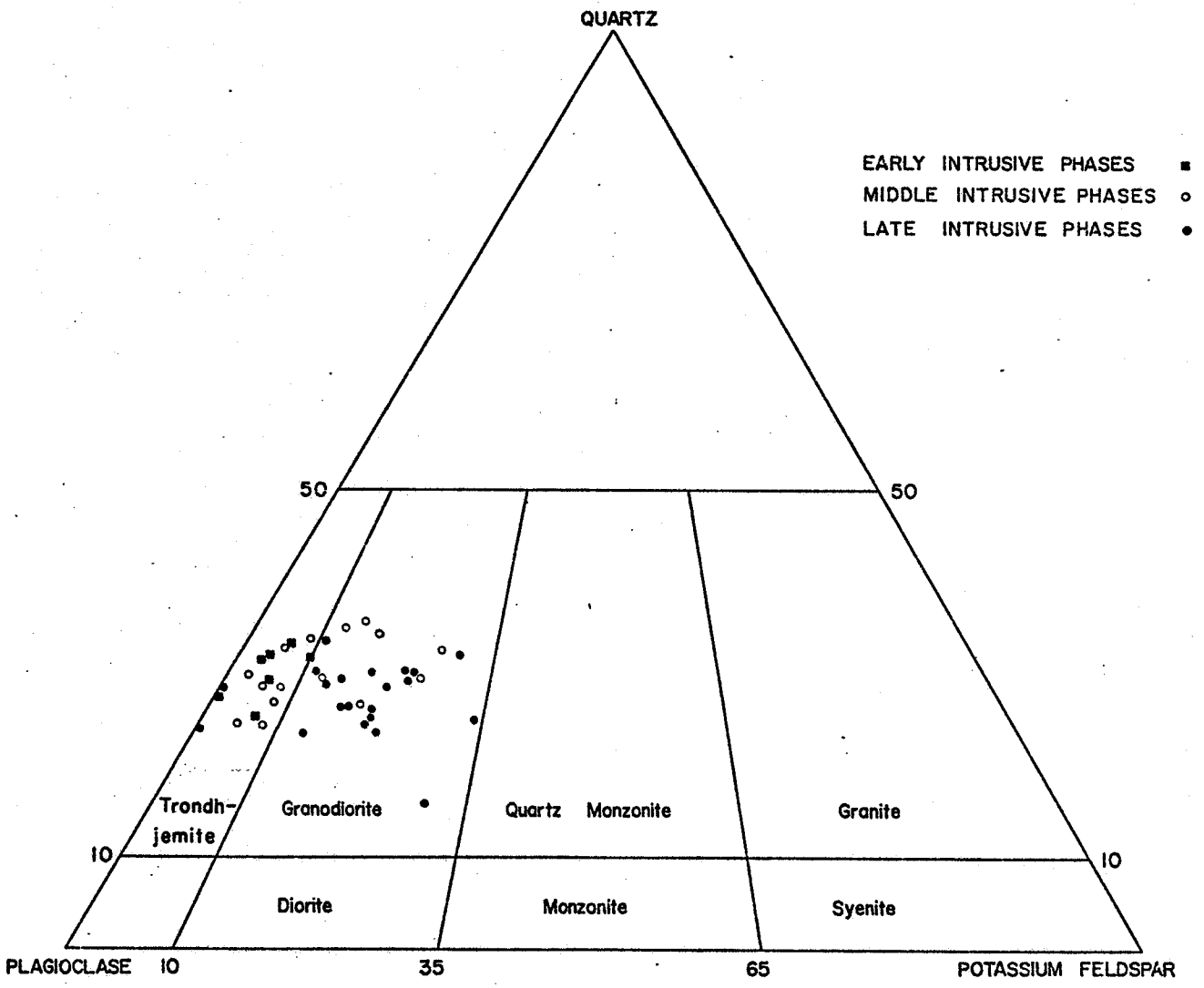

Figure 5. Normative quartz-plagioclase-potassium feldspar ternary diagram.

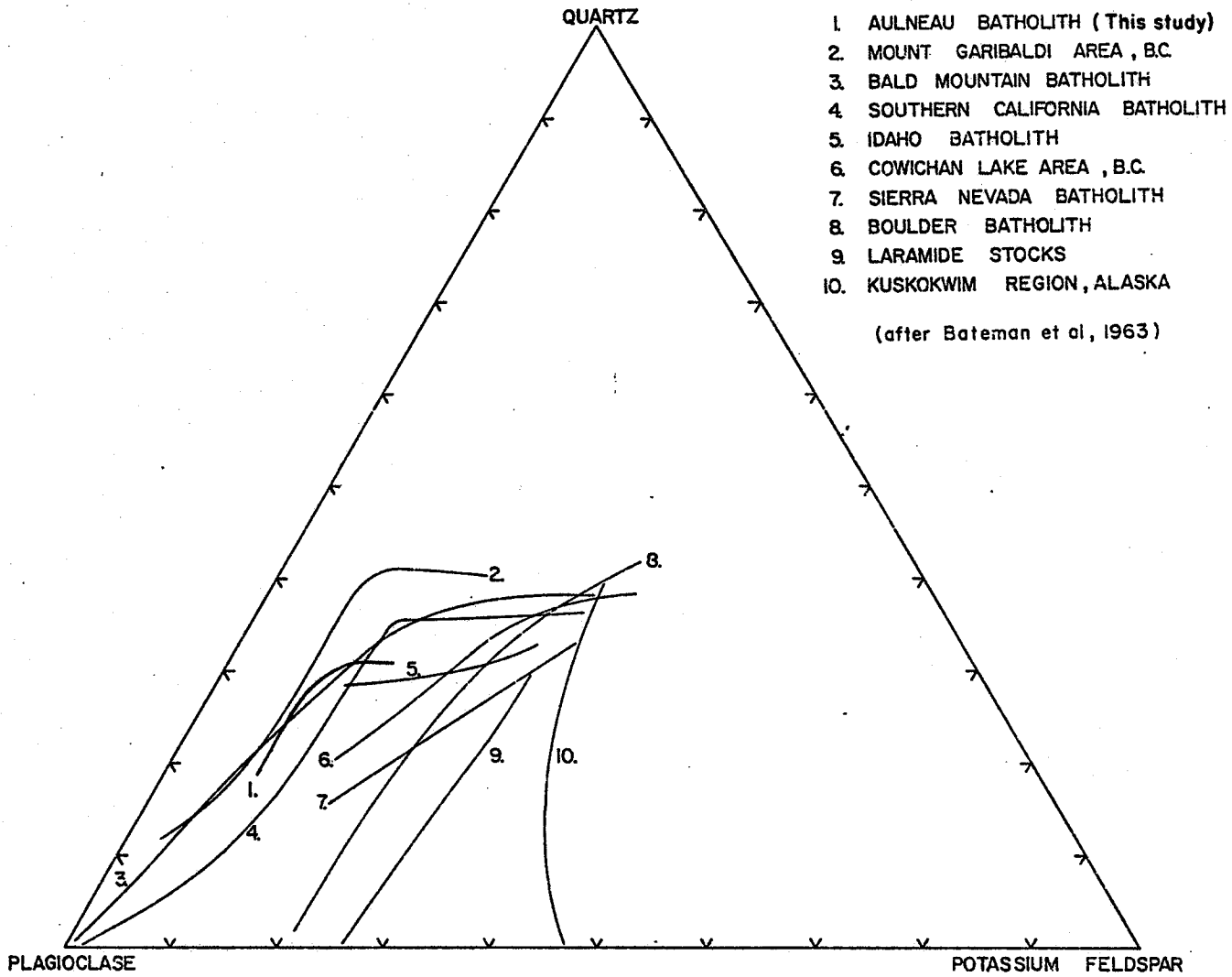

Figure 6. Normative quartz-plagioclase-potassium feldspar ternary comparison diagram.

STATISTICAL DISTRIBUTION OF THE ELEMENTS

This section presents a statistical examination of the distribution of the elements with the objective of identifying any features of the sample population which could be applied to a geologic interpretation of the data.

The size of the sample population, range, arithmetic mean and standard deviation of the major and trace elements used in this study are collated in Table 1, histograms of the major and trace elements are shown in Figures 7, 8 and 9. The sample population includes 7 samples from the early intrusive phases, 15 samples from the middle intrusive phases and 21 samples from the late intrusive phases.

Inspection of the histograms of the major elements reveals that SiO_2 has a unimodal distribution characterized by negative skewness, and that Al_2O_3, Fe_2O_3, FeO, CaO, MgO, Na_2O, K_2O, TiO_2, MnO, H_2O and CO_2 have unimodal distributions characterized by positive skewness. Histograms of the trace elements illustrate that Li, Pb, Ni, Cu, Co, Rb and Zn have unimodal distributions characterized by positive skewness. Histograms of S, Sn and Cs are not presented due to lack of data.

Major and trace element distribution data for the elements used in this study, with the exception of H_2O, S, CO_2, Zn and Sn distributions, were presented by Ahrens (1966). The major and trace element distributions of the data used in this study are in general

Table 1. Major and trace element ranges, averages and standard distributions.

Element	Number of Samples	Element Detected In	Range	Arithmetic Mean	Standard Deviation
SiO_2	43	43	64.65 - 73.10	70.80	1.96
Al_2O_3	43	43	14.14 - 17.09	15.87	0.59
Fe_2O_3	43	43	0.26 - 1.80	0.82	0.41
FeO	43	43	0.40 - 2.32	1.02	0.37
CaO	43	43	1.66 - 4.52	2.61	0.55
MgO	43	43	0.41 - 1.54	0.78	0.33
Na_2O	43	43	4.67 - 6.90	5.43	0.50
K_2O	43	43	0.85 - 2.61	1.57	0.48
TiO_2	43	43	0.17 - 0.43	0.26	0.07
P_2O_5	43	43	0.05 - 0.27	0.11	0.04
MnO	43	43	0.02 - 0.06	0.03	0.02
H_2O	43	43	0.04 - 1.46	0.59	0.23
S	43	14	0.00 - 0.01	0.00	0.00
CO_2	43	42	0.00 - 0.70	0.10	0.12
Li	43	43	15 - 58	33	9
Pb	43	43	1 - 52	13	11
Ni	43	40	0 - 38	10	8
Cu	43	43	2 - 29	12	7
Co	43	38	0 - 14	6	4
Zn	43	43	29 - 64	48	7
Rb	43	43	24 - 75	43	12
Sn	31	13	0 - 21	3	5
Cs	31	1	0 - 12	-	-

Major elements in weight percent
Trace elements in parts per million

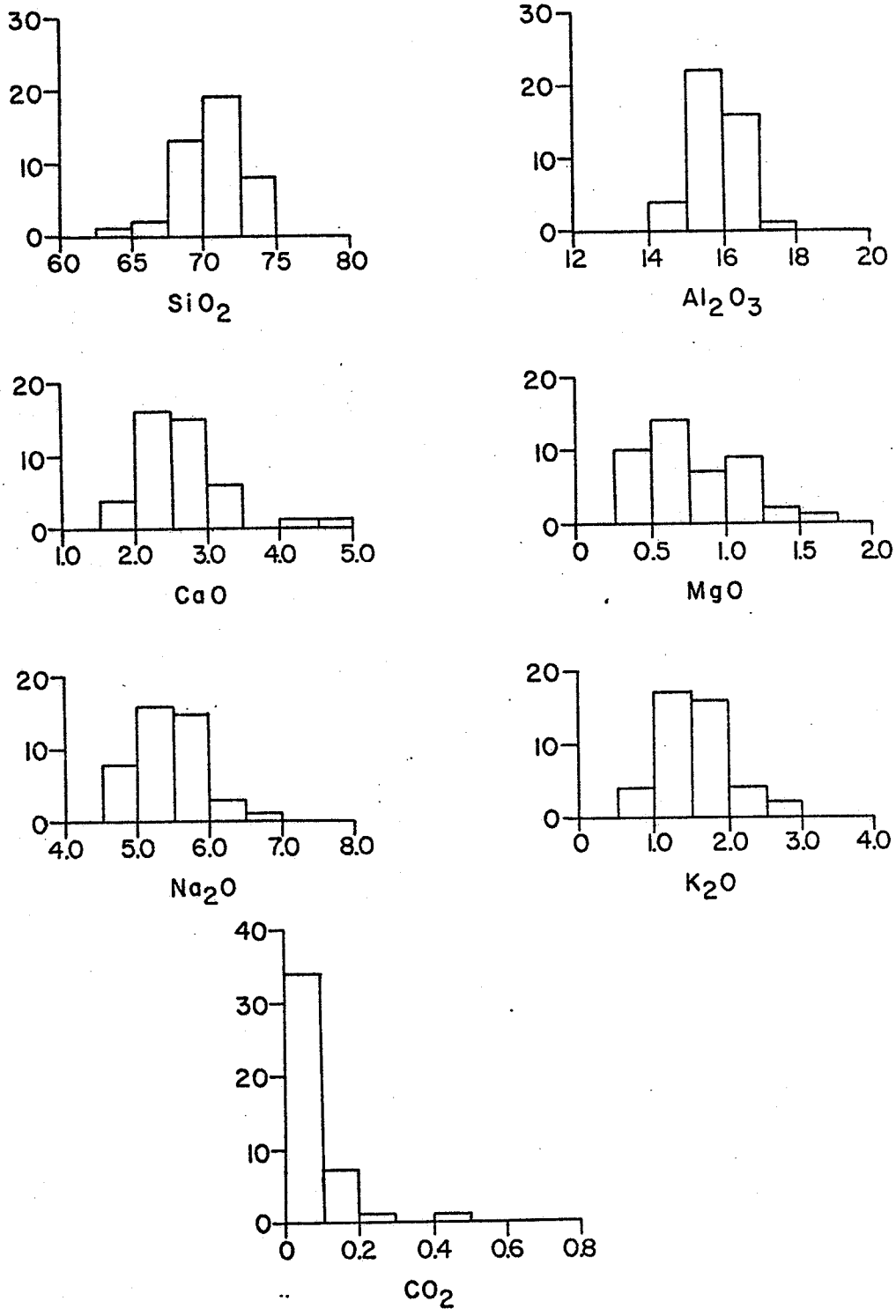

Figure 7. SiO_2, Al_2O_3, CaO, MgO, Na_2O, K_2O and CO_2 histograms.

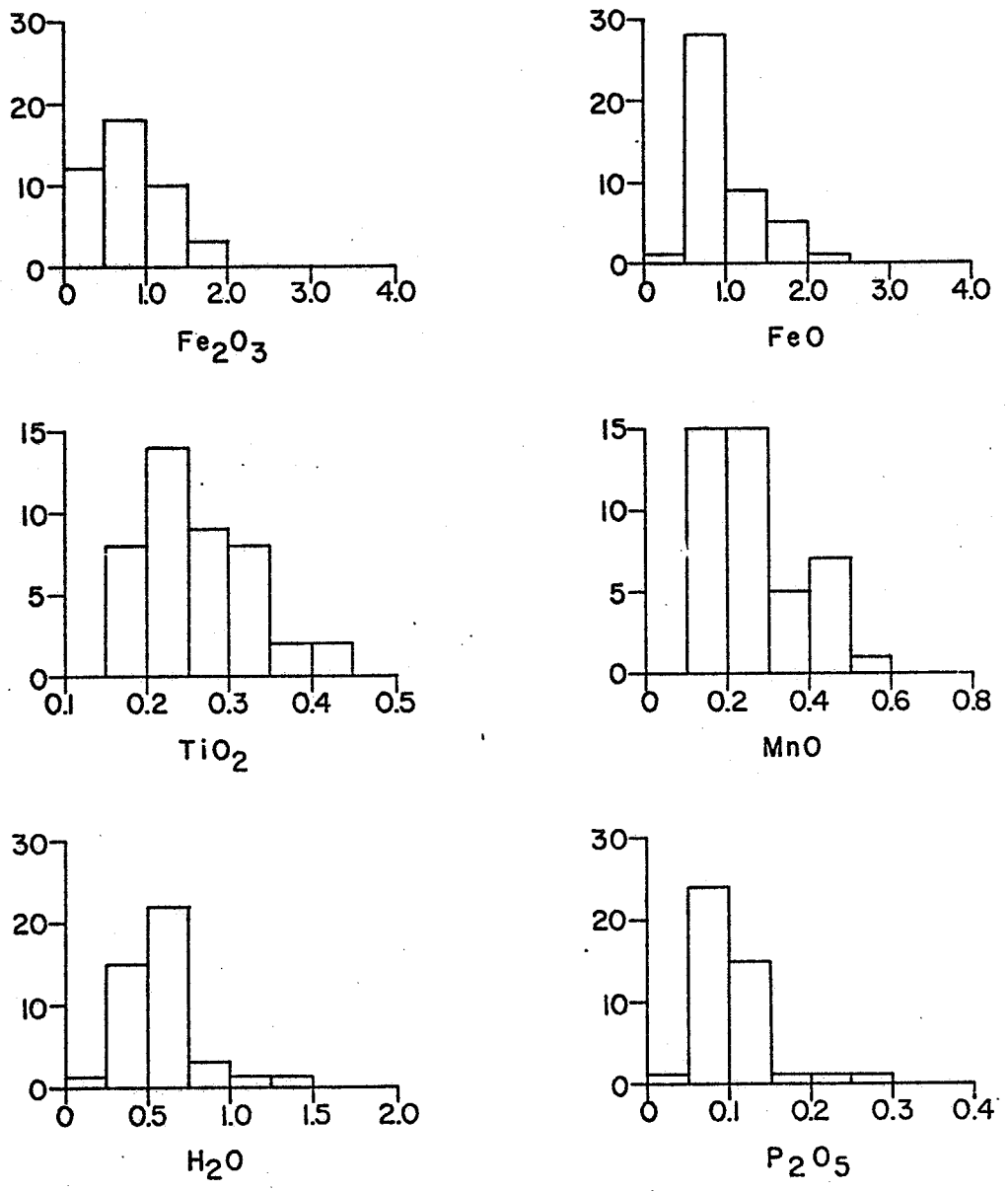

Figure 8. Fe_2O_3, FeO, TiO_2, MnO, H_2O and P_2O_5 histograms.

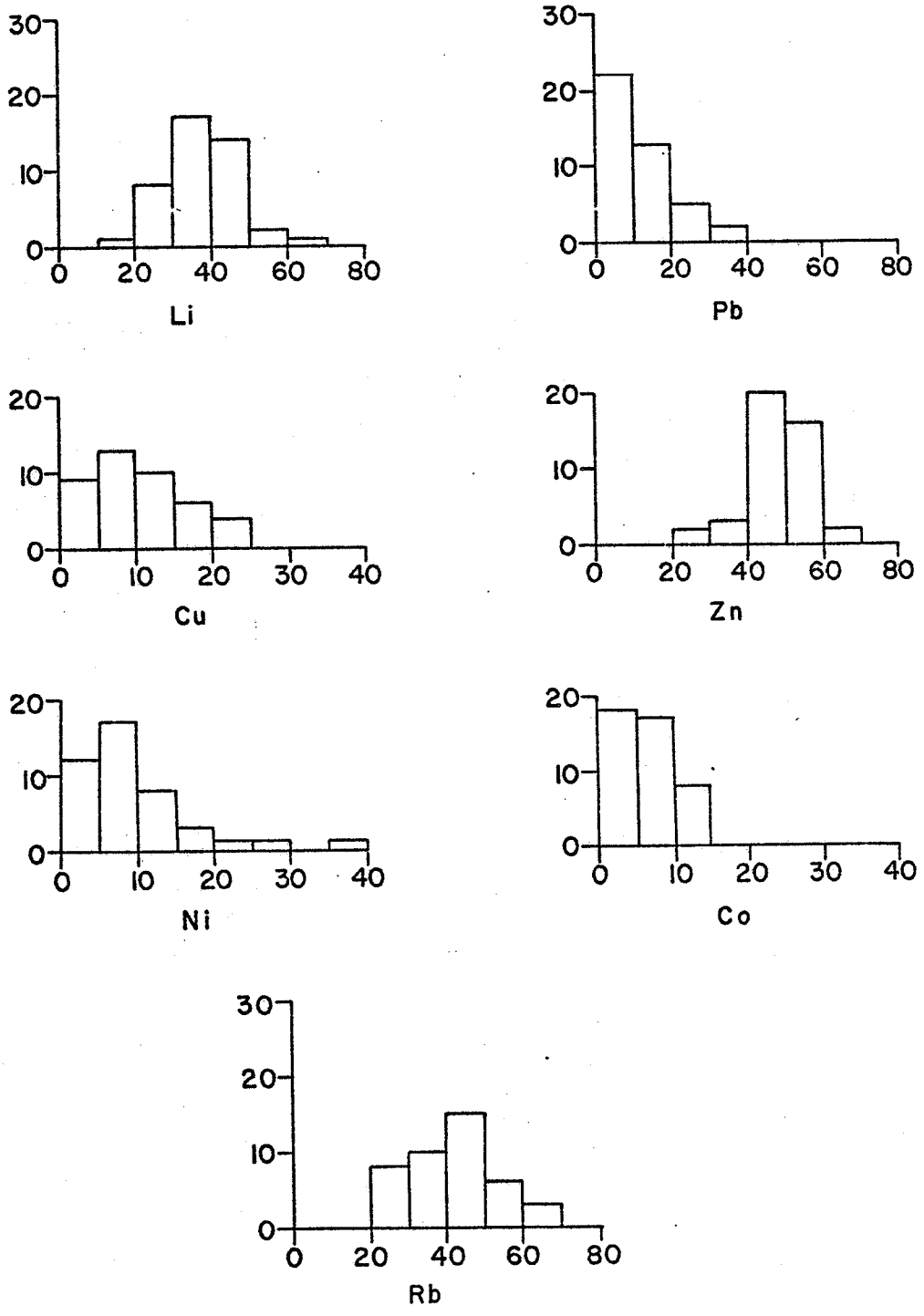

Figure 9. Li, Pb, Cu, Zn, Ni, Co and Rb histograms.

agreement with the distribution data compiled by Ahrens with the exception of K_2O. According to Ahrens K_2O shows a distinct tendency for negative skewness, as opposed to the positive skewness observed in this study. The positive skewness in the K_2O distribution may be due to the larger sub-population of higher K_2O contents in the late intrusive phases as compared to the lower K_2O values of the early and middle intrusive phases.

Ahrens (1966) suggested that the distribution of the natural logarithms of the major and trace element concentrations are normal, and that skewed unimodal distributions of the arithmetic values of the elemental concentrations are lognormal.

The Kolmogorov-Smirnov statistic provides a means of testing whether a set of observations are from some completely specified continuous distribution (Lilliefors, 1967), and is particularily useful in testing small populations. In a sample of N observations, one determines $D = \max_X \left|F^*(X)-S_N(X)\right|$, where $S_N(X)$ is the cumulative distribution function and $F^*(X)$ is the cumulative normal distribution with $\mu = X$, the sample mean, and $\sigma^2 = s^2$, the sample variance, defined with denominator n - 1. If the value of D exceeds the critical value of D, the hypothesis that the observations are from a normal population is rejected.

The distributions of the natural logarithmic transformations of the major and trace element concentrations were tested by the Kolmogorov-Smirnov test (Appendix 5). At the 90% confidence level the distributions of P_2O_5, MnO, CO_2, Ni and Co are rejected as lognormal. Application of the Kolmogorov-Smirnov test to the arithmetic major and trace element concentration distributions indicates that

the distributions of Fe_2O_3, FeO, MgO, TiO_2, P_2O_5, MnO, CO_2, Pb, Ni and Cu are rejected as normal at the 90% confidence level.

Irrespective of the irregular distribution of samples with regard to the number of samples from the early, middle and late intrusive phases, the distribution of the elements represent unimodal distributions. The mutual exclusion of P_2O_5, MnO, CO_2 and Ni from either normal or lognormal distributions indicates that they represent some unspecified unimodal distributions. The distribution of the other elements studies appears lognormal. The distribution data of the sample population suggests that the Aulneau batholith is amenable to interpretation as a single chemical system.

MAJOR ELEMENT GEOCHEMISTRY

Relationships between the major elements of a granitic body serve to establish the chemical affinity of that body. Establishing the nature of the chemical affinity puts important petrochemical constraints upon the mechanisms which may be employed to derive the parental magma.

The subalkaline character of the Aulneau batholith is illustrated in Figure 10, the total $Na_2O + K_2O - SiO_2$ diagram. The samples are well within the subalkaline field as defined by Irvine and Baragar (1971). The early and middle intrusive phases show an increase in $Na_2O + K_2O$ with increasing SiO_2, and a considerable overlap in their compositional fields. The late intrusive phases show a greater total $Na_2O + K_2O$ content than the early and middle intrusive phases, and a decrease in the total $Na_2O + K_2O$ with increasing SiO_2.

Figure 11, the $Na_2O + K_2O - FeO - MgO$ ternary diagram is used in this study to distinguish between the two subalkaline igneous series; the tholeiitic and calc-alkaline rock series. The early, middle and late intrusive phases exhibit a strong collinear relationship and show a trend of increasing $Na_2O + K_2O$ at a constant FeO/MgO ratio, this relationship is characteristic of subalkaline rocks of the calc-alkaline series. In Figure 12 the trend of Aulneau batholith illustrated in Figure 11 is compared with trends from other calc-alkaline batholiths, a tholeiitic trend, and the field boundary

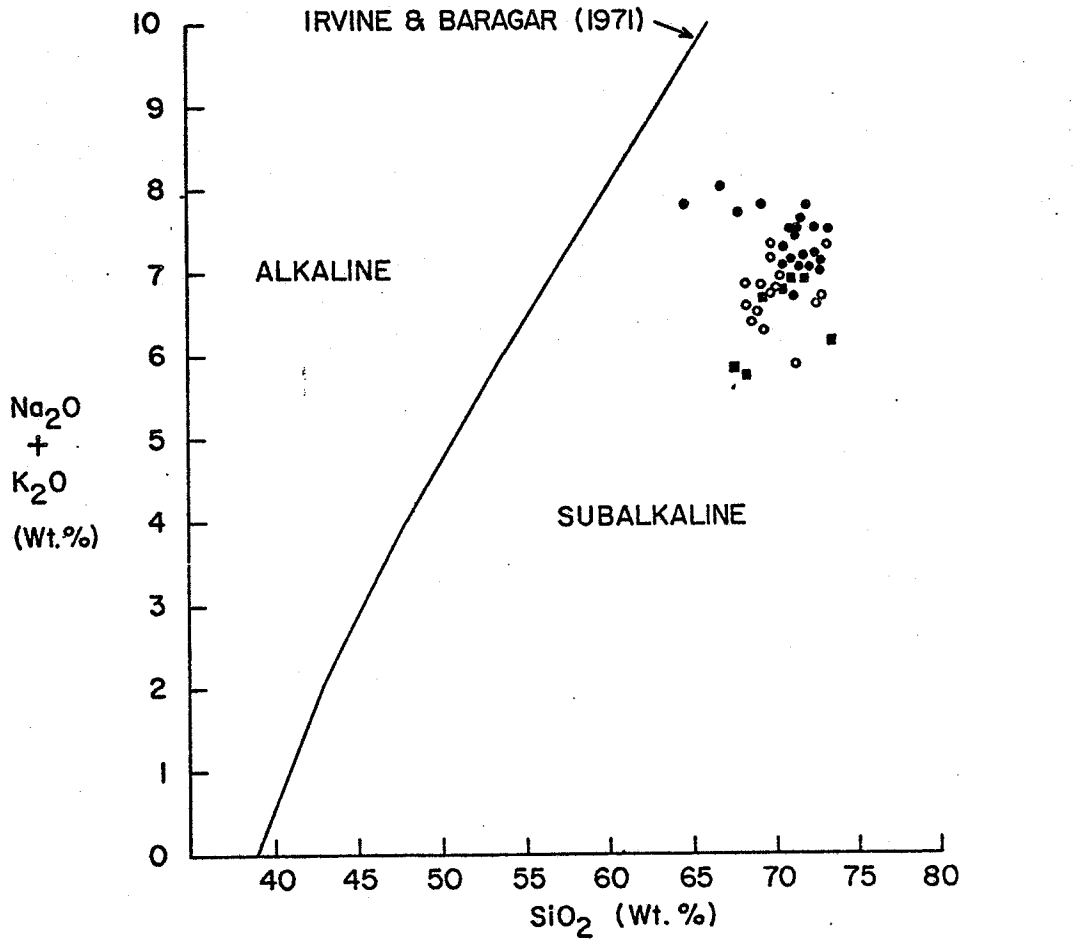

Figure 10. $Na_2O + K_2O - SiO_2$ diagram.

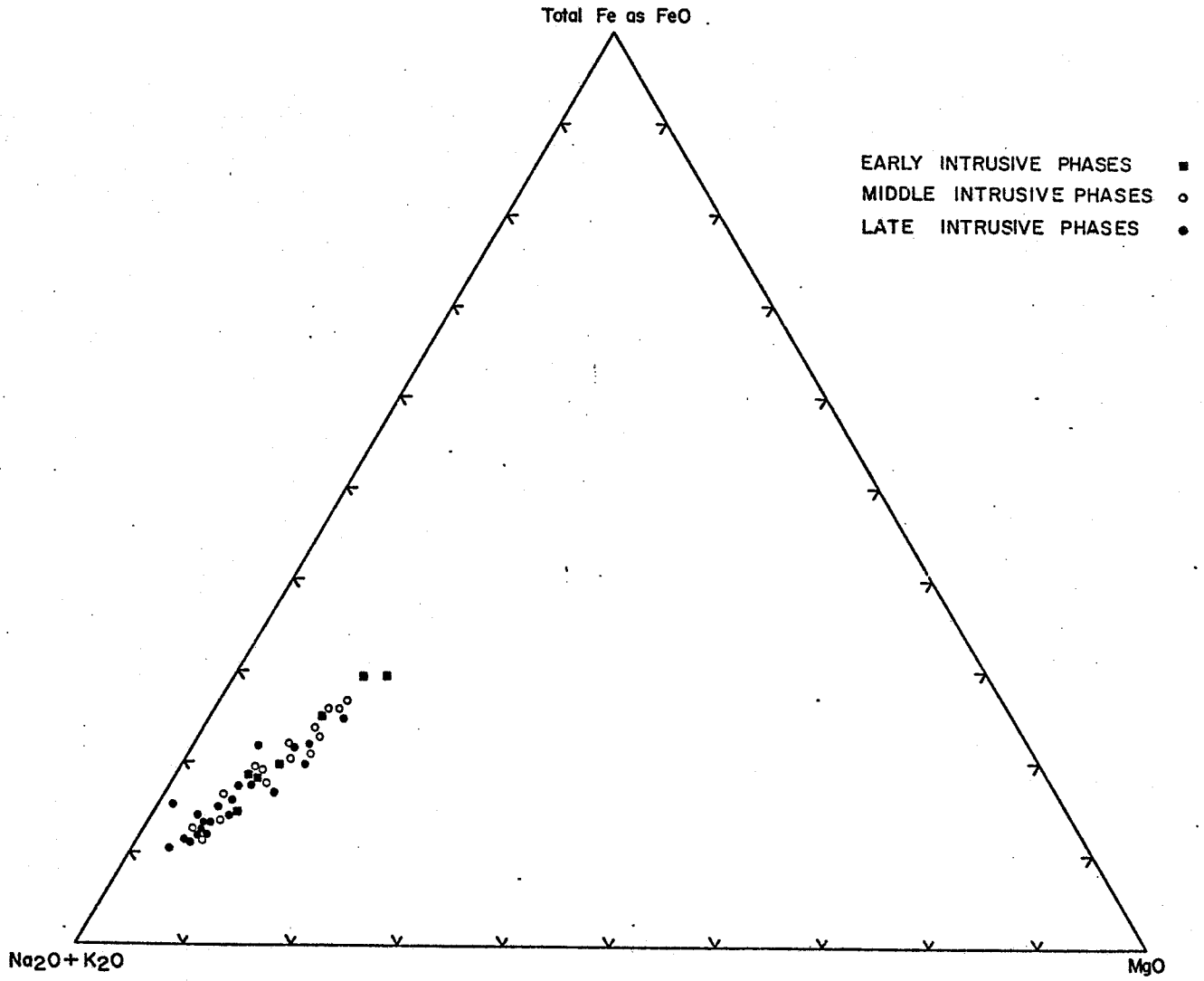

Figure 11. $Na_2O + K_2O$ - FeO - MgO ternary diagram.

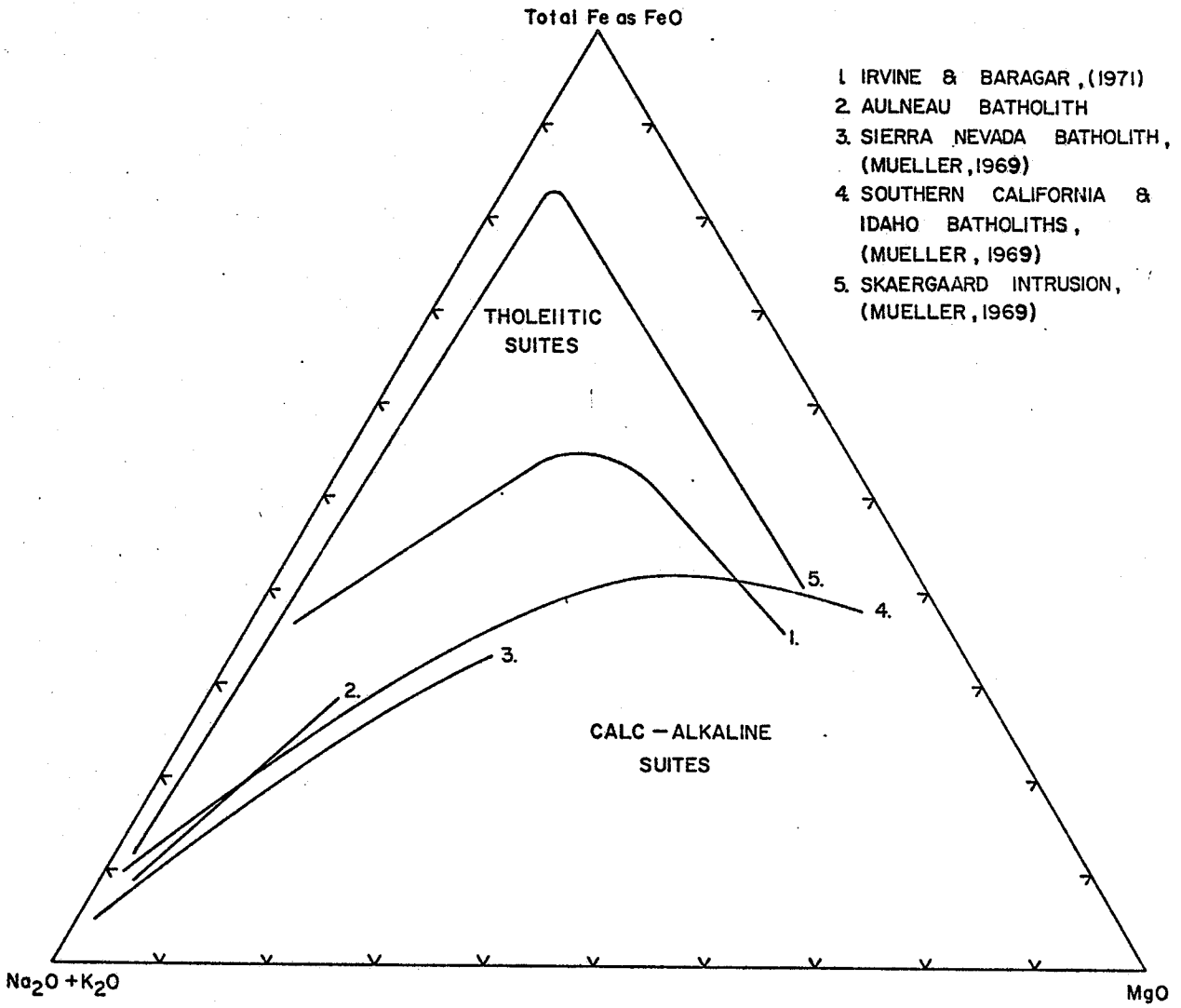

Figure 12. $Na_2O + K_2O$ - FeO - MgO ternary trend comparison diagram.

between the tholeiitic and calc-alkaline series as established by Irvine and Baragar (1971). Figure 12 illustrates that the Aulneau batholith has a trend similar to the trends of other calc-alkaline batholiths, but that it is limited to a smaller compositional field.

In Figure 13, the Na_2O - K_2O - CaO ternary diagram, the Na_2O/CaO ratios of the early intrusive phase samples define a trend of increasing Na_2O at a relatively constant K_2O content. The Na_2O/CaO ratios of the middle intrusive phase samples weakly define a trend of increasing Na_2O with a corresponding increase in the K_2O/Na_2O ratio. The K_2O/Na_2O ratios of the late intrusive phase samples show a trend of increasing K_2O at a relatively constant Na_2O/CaO ratio.

The K_2O/Na_2O ratios of the batholith range between 0.18 and 0.24 in the early intrusive phase, 0.20 and 0.45 in the middle intrusive phase and 0.14 and 0.52 in the late intrusive phase. The average K_2O/Na_2O ratio is 0.29.

The major element geochemistry indicates that the Aulneau batholith is subalkaline and that it is characterized by a relatively constant FeO/MgO ratio with respect to increasing total alkalies and increasing SiO_2, and an increasing K_2O/Na_2O ratio with respect to increasing SiO_2 content. These features indicate that the Aulneau batholith is of calc-alkaline affinity.

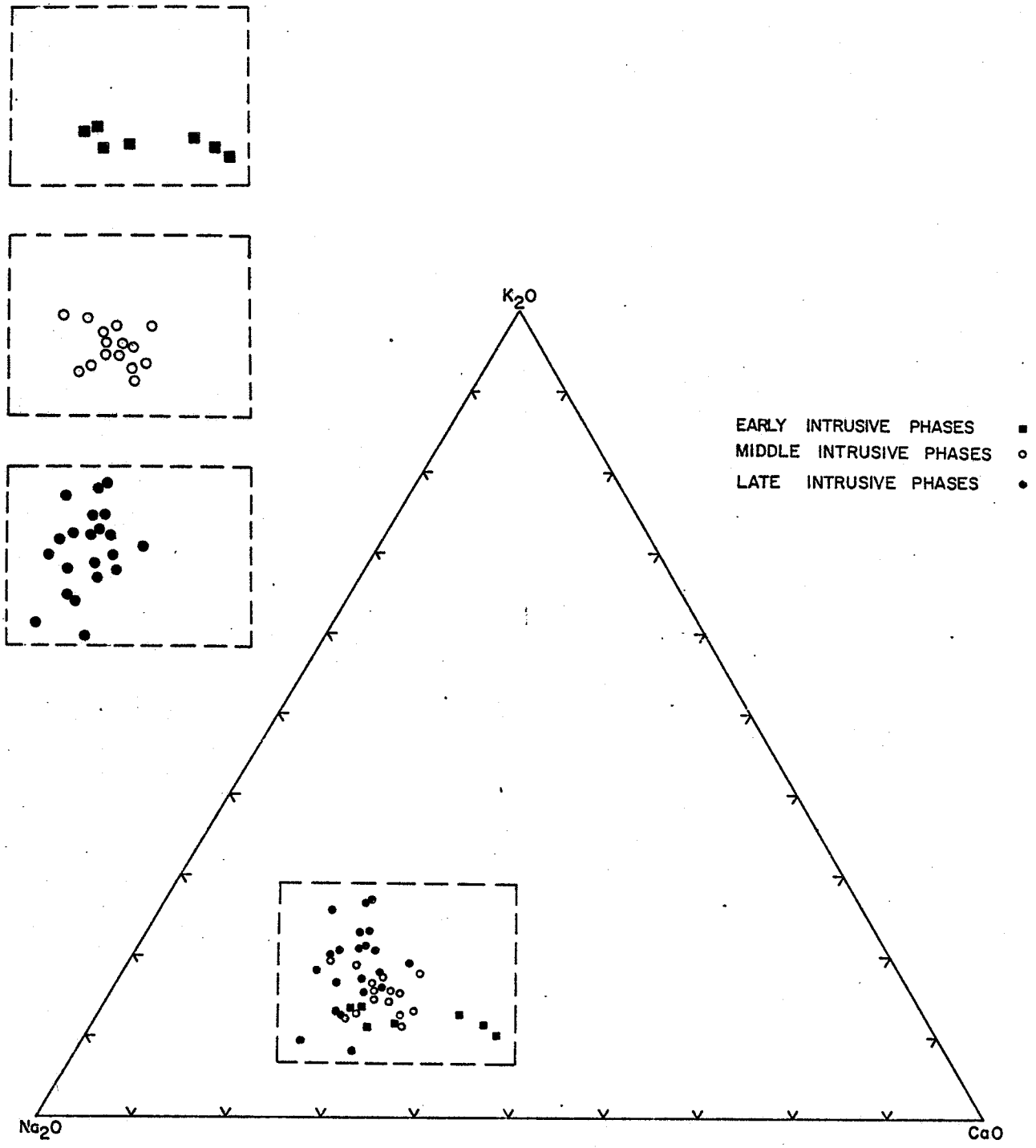

Figure 13. Na_2O - K_2O - CaO ternary diagram.

LARSEN VARIATION DIAGRAMS

The chemical analyses of the Aulneau batholith samples are plotted on Larsen variation diagrams in Figures 14, 15, 16, 17, 18 and 19. The Larsen differentiation index is (1/3 SiO_2 + K_2O) - (Total Fe as FeO + CaO + MgO) and was proposed by Larsen (1938) to show the correlation of chemistry with the presumed order of magmatic evolution (Carmichael, Turner and Verhoogen, 1974). Larsen differentiation indices in this study vary from 14.5 to 23.5, the samples from the early, middle and late intrusive phases show a considerable overlap in their Larsen differentiation indices. The average Larsen differentiation indices for the early, middle and late intrusive phases show a progressive increase from 18.3 to 19.4 and 20.8 respectively. Treatment of the data by Larsen variation diagrams may mask possible reversals in magma evolution within the early, middle and late intrusive phases, however, the data base is not sufficiently complete to investigate the chemistry of the individual intrusive phases.

Due to the fact that the samples have a narrow range of Larsen differentiation indices the trends of the major and trace elements are amenable to treatment as a straight line. Linear regression analysis of the early, middle and late intrusive phases in addition to the total sample population was performed. Numerical parameters of the regression lines are contained in Appendix 7.

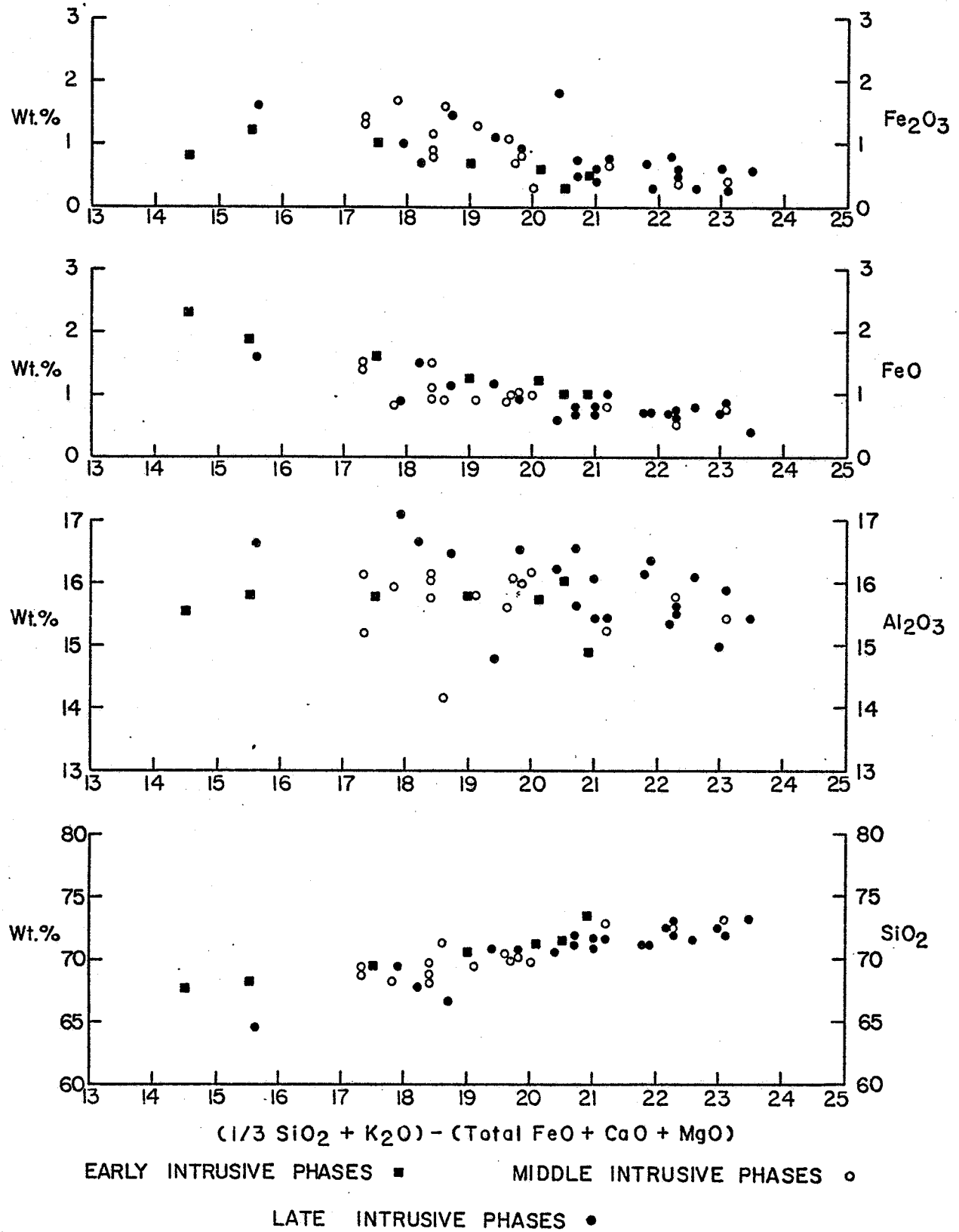

Figure 14. SiO_2, Al_2O_3, FeO and Fe_2O_3 Larsen variation diagrams.

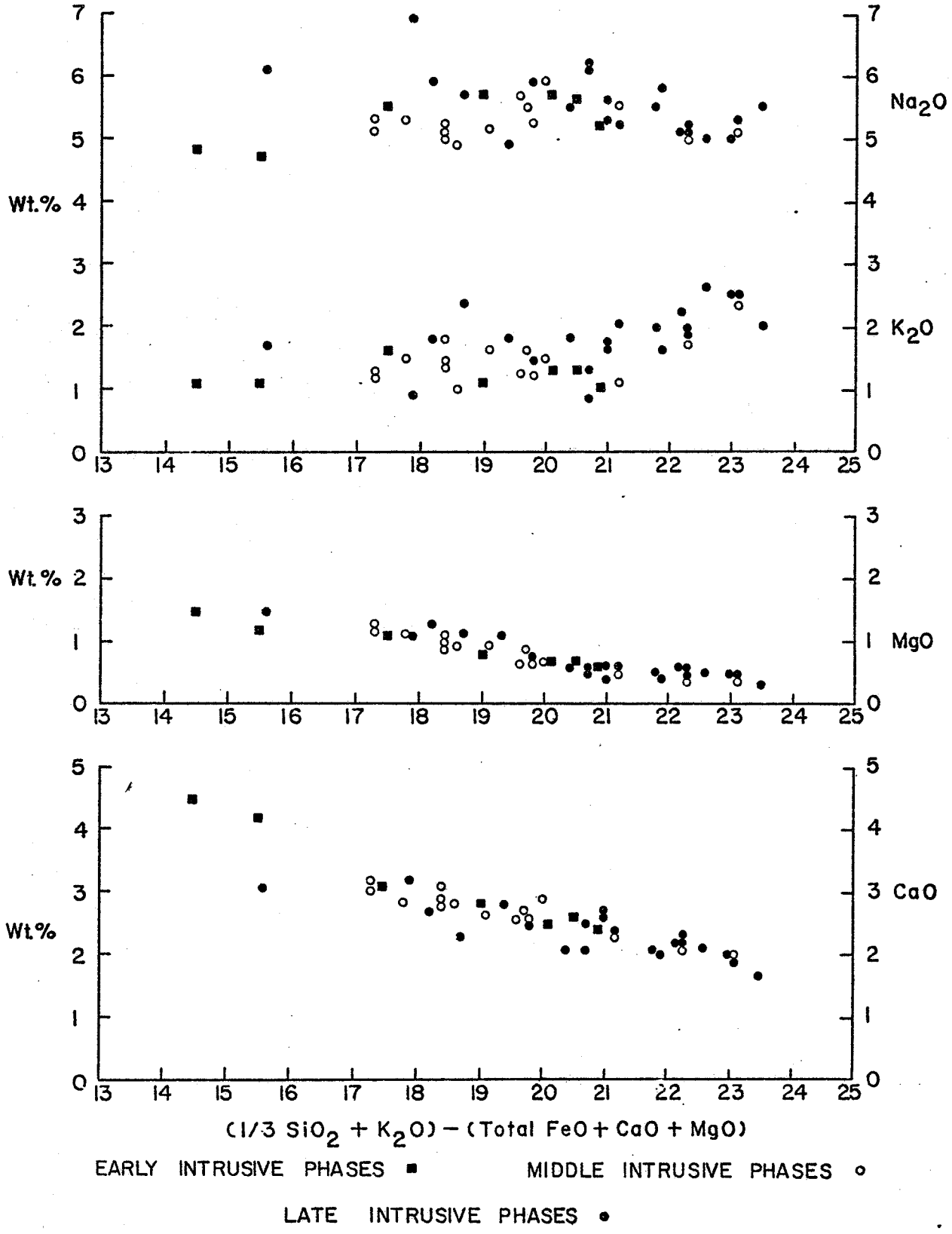

Figure 15. CaO, MgO, K_2O and Na_2O Larsen variation diagrams.

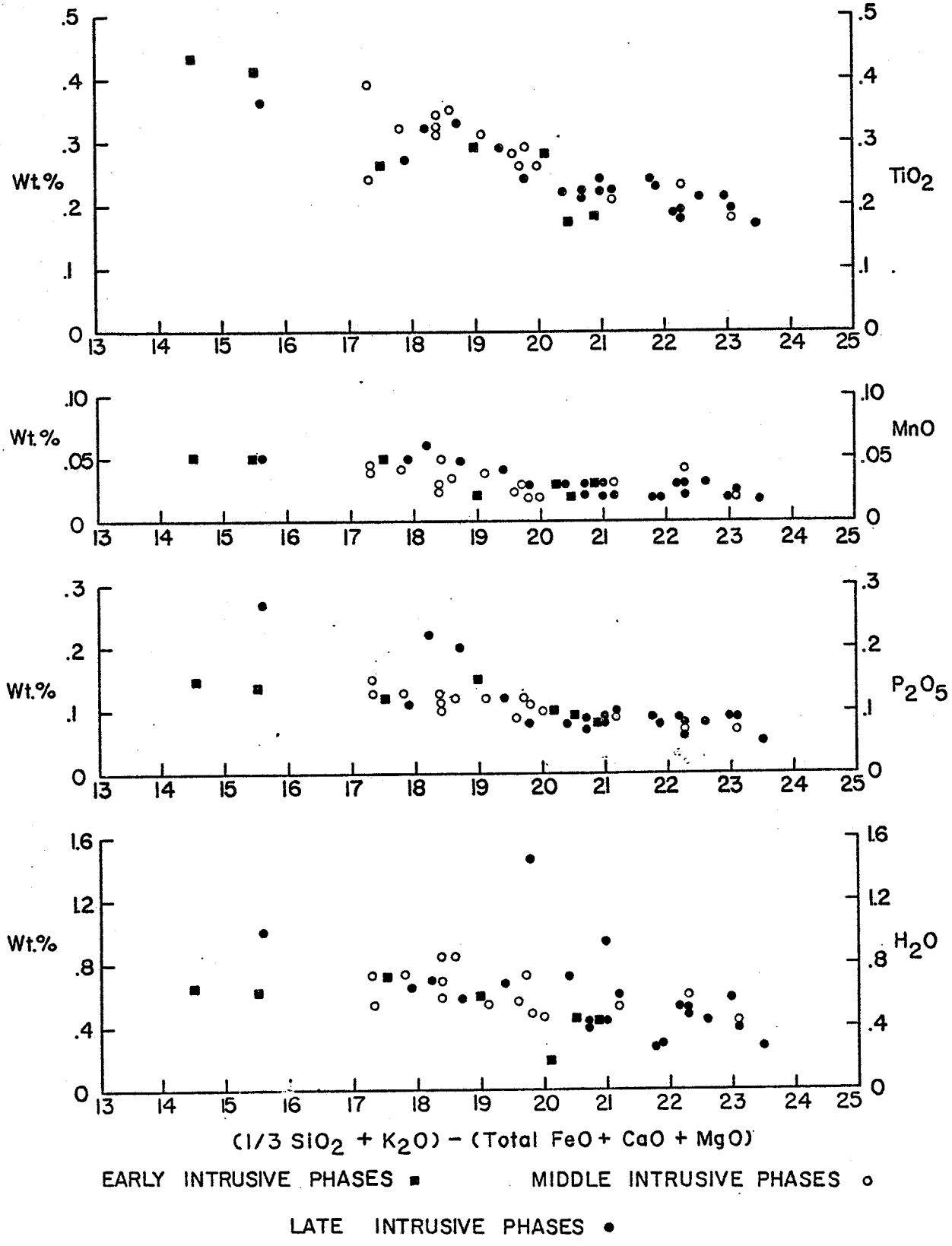

Figure 16. TiO_2, MnO, P_2O_5 and H_2O Larsen variation diagrams.

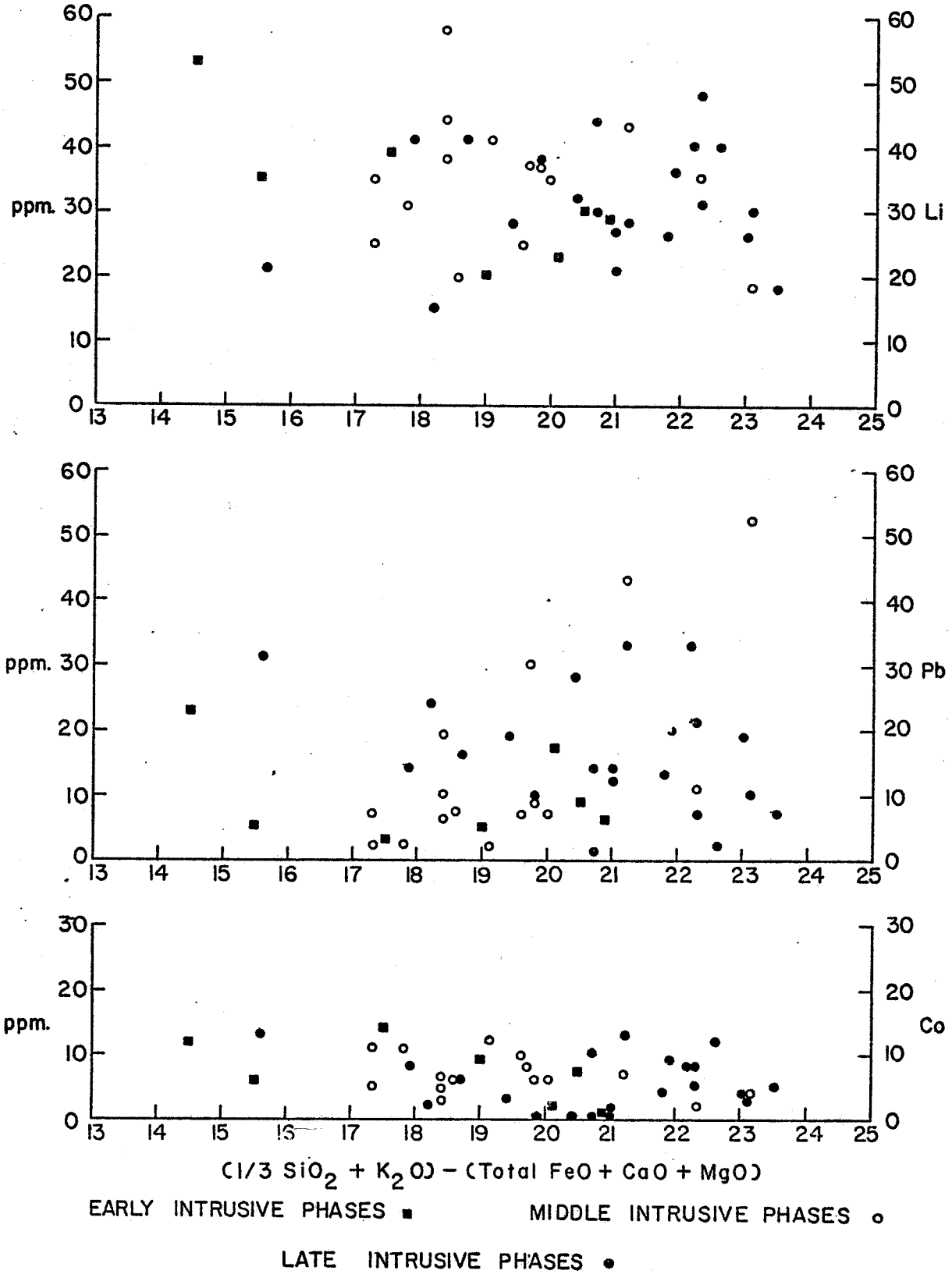

Figure 17. Li, Pb and Co Larsen variation diagrams.

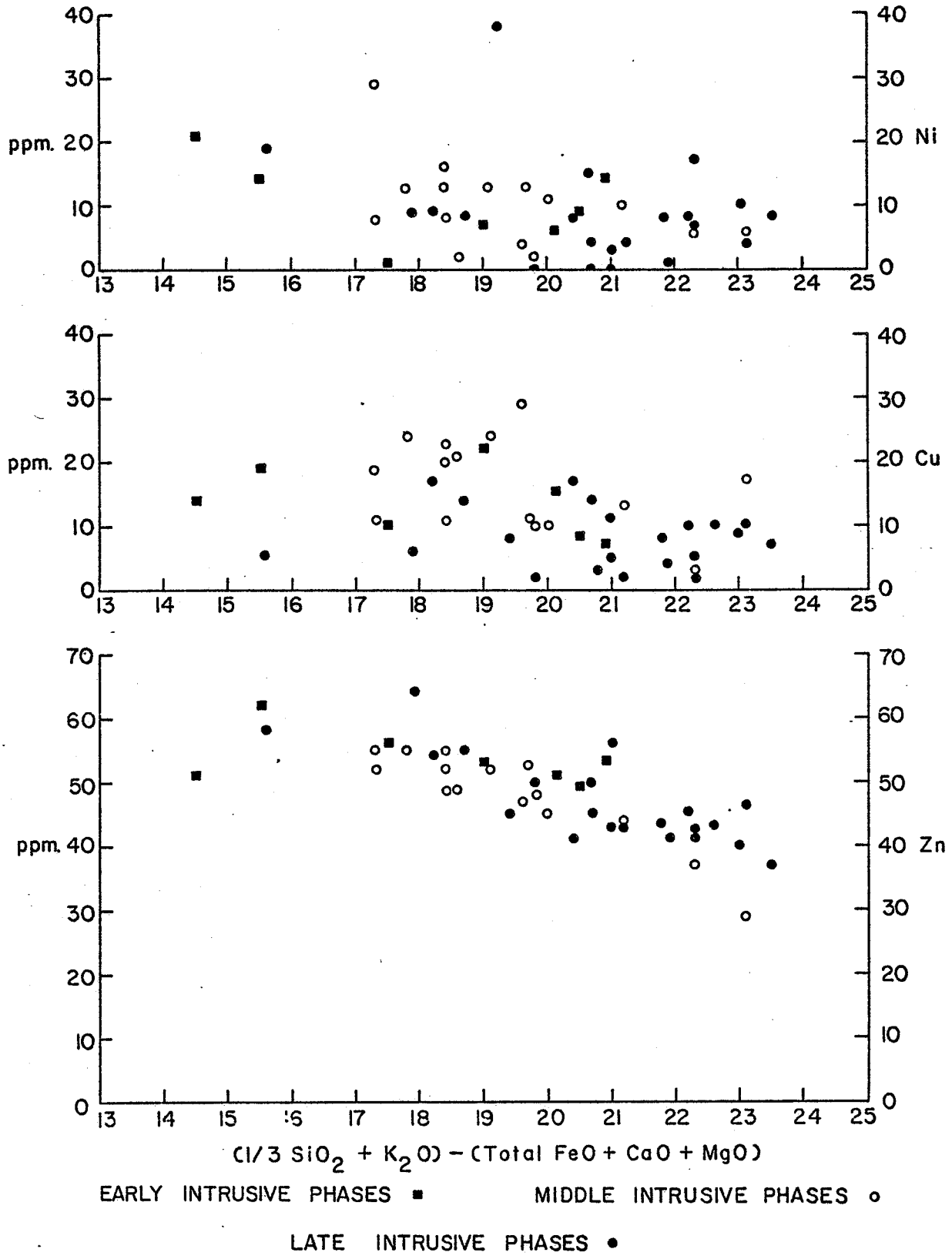

Figure 18. Ni, Cu and Zn Larsen variation diagrams.

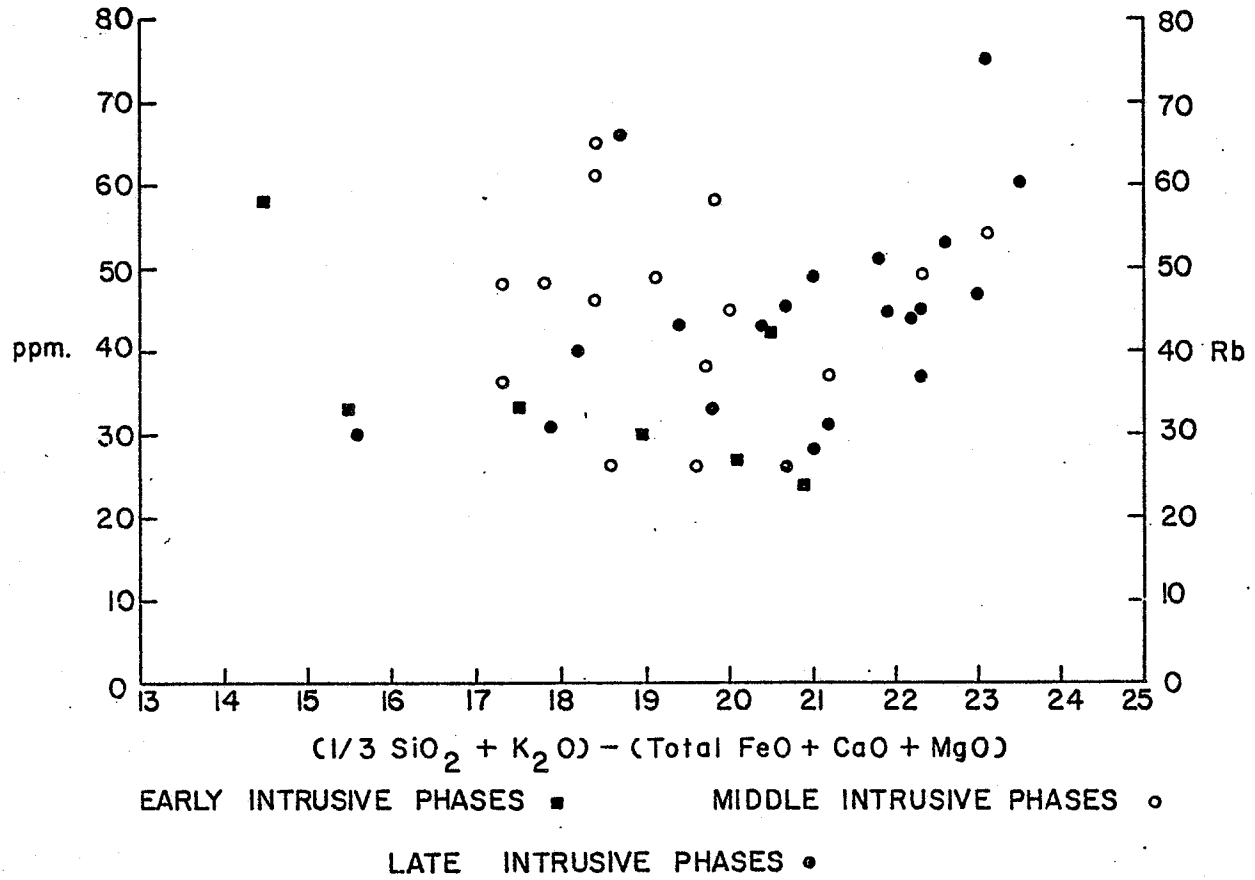

Figure 19. Rb Larsen variation diagram.

SiO_2 (Figure 14) and K_2O (Figure 15) both show trends of increasing concentration with increasing Larsen differentiation indices. Within the SiO_2 and K_2O variation diagrams the early, middle and late intrusive phases all illustrate trends of increasing concentration.

Na_2O (Figure 15) shows a very weak overall trend of decreasing concentration with increasing Larsen differentiation indices. The early and middle intrusive phases exhibit a trend of increasing concentration with increasing Larsen differentiation indices. The late intrusive phases illustrate a well defined trend of decreasing Na_2O concentration with increasing Larsen differentiation indices.

Al_2O_3, Fe_2O_3 and FeO (Figure 14), CaO and MgO (Figure 15), TiO_2, MnO, P_2O_5 and H_2O (Figure 16) show overall trends of decreasing concentration with increasing Larsen differentiation indices. The overall trends are consistent with trends of decreasing concentration exhibited by the early, middle and late intrusive phases.

The overall trends of Li and Co (Figure 17), Ni, Cu and Zn (Figure 18) all indicate decreasing concentration with increasing Larsen differentiation indices. The early and middle intrusive phase lithium concentrations show trends of decreasing concentration with increasing Larsen differentiation indices, late intrusive phase lithium values show a trend of increasing concentration with increasing Larsen differentiation indices. Ni, Cu, Co and Zn all show trends of decreasing concentration with increasing Larsen differentiation indices with respect to the trends by the early, middle and late intrusive phases.

Pb (Figure 17) shows an overall trend of increasing concentration with increasing Larsen differentiation indices. In the early

and late intrusive phases Pb shows a trend of decreasing concentration with increasing Larsen differentiation indices. Rb shows a trend of increasing concentration with Larsen differentiation indices in the early and late intrusive phases (Figure 19), in the middle intrusive phases the Rb trend decreases. The overall Rb trend increases with Larsen differentiation indices.

Nockolds and Allen (1953) investigated the behaviour of selected major and trace elements in calc-alkaline igneous rock series; major and trace element data were presented in parts per million and a modified Larsen differentiation index (1/3 Si + K) - (Ca + Mg) was used. The overall trends they observed are comparable with the trends observed in this study, however the former did not present data for manganese, water, phosphorus, copper and zinc.

Nockolds and Allen (1953) observed that silicon and potassium both increased in abundance with increasing positive values of the modified Larsen differentiation index, and that aluminum, calcium, magnesium, titanium and iron decrease in abundance with increasing positive values of the modified Larsen differentiation indices. They also observed that in some calc-alkaline igneous rock series sodium increased in concentration until it reached a feeble maximum in the intermediate members of a series, whereas in some series characterized by lower potassium content the sodium showed a small but steady rise throughout the series. The overall trend of Na_2O in the Aulneau batholith is one of increasing concentration with increasing Larsen differentiation indices, however the early and middle intrusive phases show a trend of increasing concentration of Na_2O and the late intrusive phases show a trend of decreasing Na_2O. The behaviour of

Na_2O in this study may be analogous to the behaviour cited by Nockolds and Allen for sodium in calc-alkaline igneous rock series that are characterized by higher potassium contents regardless of the low potassium content of the Aulneau batholith.

Nockolds and Allen (1953) observed that Ni and Co decreased in concentration and that Li, Rb and Pb increased in concentration with increasing positive values of the Larsen differentiation indices. Similar relationships for the trace elements are observed in this study with the exception of Li which shows a very weakly defined trend of decreasing concentration.

The presumed order of magmatic evolution as shown by an increase in Larsen differentiation indices is obscured in this study because the three major phases embody nineteen individual phases which overlap in composition and show reversals in composition. However, if the Larsen variation diagrams are considered in terms of a general differentiation trend, the variations in individual major and trace elements are compatible with the calc-alkaline character of the batholith.

TRACE ELEMENT GEOCHEMISTRY

Emperical rules for the distribution of trace elements during magmatic activity were formulated by Goldschmidt (1937). Based on a simple ionic model he suggested that: (1) if two ions have the same ionic radius and the same charge, they will enter into solid solutions in a given mineral in amounts roughly proportional to their abundances, (2) if the two ions have similar radii and the same charge, the smaller ion will be preferentially concentrated in the solid phase, (3) if two ions have similar ionic radii but different charges, the ion with the higher charge will enter the crystal structure preferentially. Exceptions to these rules were attributed to the effects of covalent bonding.

Ringwood (1955) modified Goldschmidts' rules by considering the influence of electronegativity. He suggested that for two ions with similar charges and ionic radii, the ion with the lower electronegativity will be preferentially incorporated into the crystal structure because of the stronger and more ionic bond.

Nockolds (1966) considering bond energy criteria proposed that: (1) when two cations of the same valency are capable of substitution in a crystal lattice, the cation having the greater relative total bonding energy will be incorporated preferentially, (2) when two cations of different valency, involving coupled substitution in a crystal lattice, that substitution will take place preferentially

whose sum of relative bonding energies is the greater.

Burns and Fyfe (1967) reviewed the preceeding rules used to explain the distribution of trace elements. They presented convincing arguments based on consideration of homogeneity, phase equilibria, thermodynamic factors, ionic radii, electronegativity, melting points and heats of formation, that these rules are inadequate to explain the distribution of all elements, especially the transition metals.

Although there is considerable debate as to the factors which control trace element distribution during magmatic activity, the data of the present study were considered in terms of the Goldschmidt and Ringwood rules.

Lithium

The small ionic radius of Li^+ (0.68 A) with respect to the ionic radii of other alkali elements (Na^+, 0.97 A; K^+, 1.33 A) prevents it from occupying similar lattice positions and as a result Li^+ enters six-fold co-ordination positions (Taylor, 1965). The similarity in ionic radii between Li^+ and Mg^{2+} (0.66 A) suggests that Li^+ may substitute for Mg^{2+} (Taylor, 1965).

The relationship between Li and MgO in the Aulneau batholith is illustrated in Figure 20. Linear regression analysis of Li and MgO indicates that there is negligible correlation ($r = 0.094$) between the two components.

The distribution of lithium was investigated by Horstman (1957), average lithium contents for granitic rocks and diorites were reported as 40 and 24 parts per million respectively. The average lithium concentration of the Aulneau batholith of 33 parts per

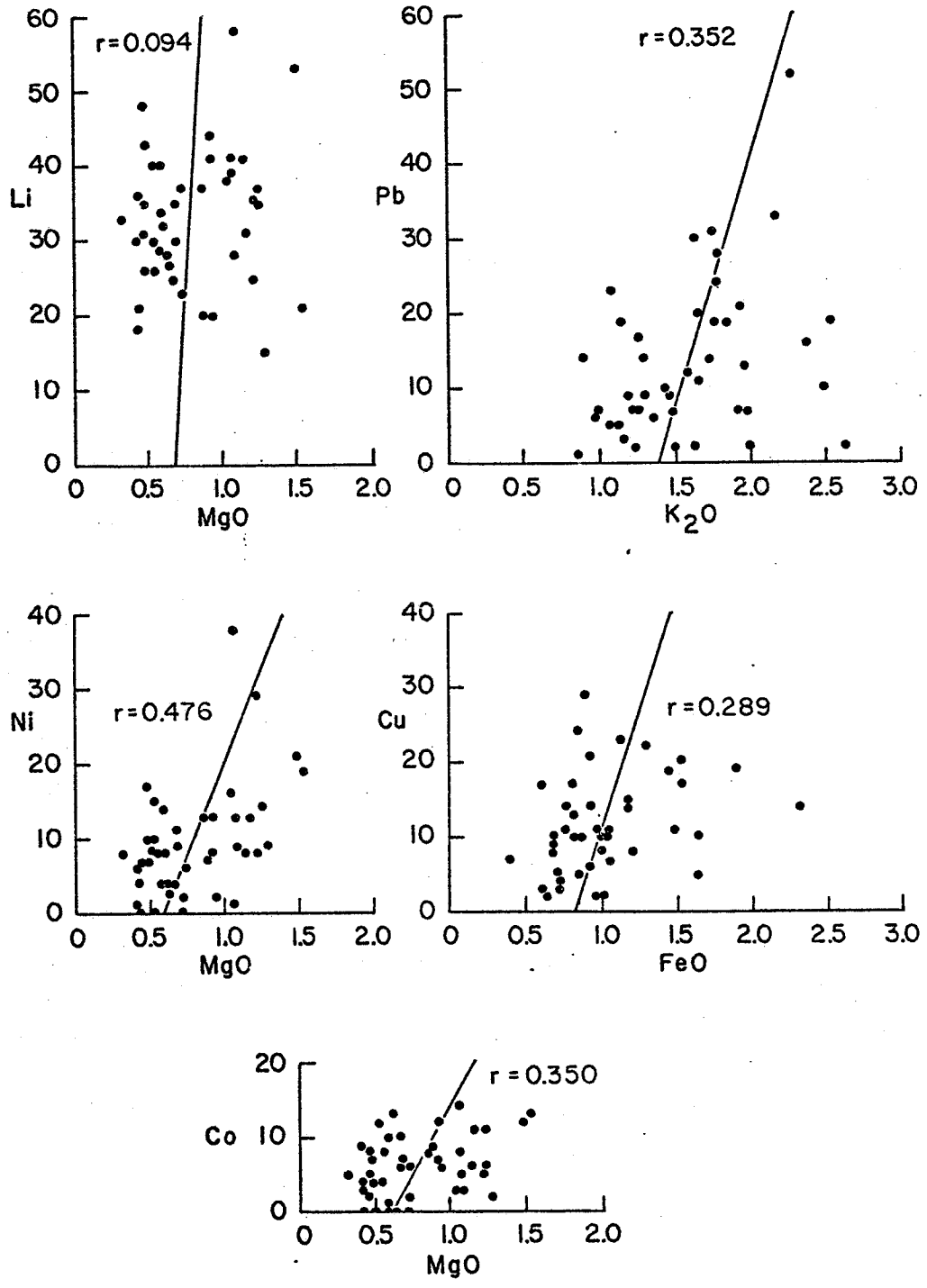

Figure 20. Li-MgO, Pb-K_2O, Ni-MgO, Cu-FeO and Co-MgO scatter diagrams.

million is intermediate between the values reported by Horstman for granitic rocks and diorites.

Lead

As a result of its higher charge Pb^{2+} should be concentrated relative to K^{+} in early potassium-bearing minerals, however the Pb-O bond is more covalent than the K-O bond and therefore Pb^{2+} tends to be concentrated in residual magmas (Ringwood, 1955).

The ionic radius of Pb^{2+} (1.2 A) is intermediate between the ionic radii of Ca^{2+} (0.99 A) and K^{+} (1.33 A) and can be expected to occur in potassium feldspars and micas substituting for K^{+}, and for Ca^{2+} in plagioclase, apatite and other minerals containing large lattice sites (Taylor, 1965). Taylor also suggested that Pb^{2+} should enter late Ca^{2+} lattice positions because of the larger size of the Pb^{2+} ion and the more covalent character of the Pb-O bond as opposed to the Ca-O bond.

The relationship between Pb and K_2O in the Aulneau batholith is shown in Figure 20. The correlation coefficient for Pb and K_2O is low ($r = 0.352$).

The average Pb content of the samples analyzed for this study is 13 parts per million. The Opemisca pluton granodiorites (Wolhuter, 1971) and the Lake St. Joseph granodiorites (Vollrath, 1964) contain 10 and 13 parts per million Pb respectively. Comparison of the Aulneau batholith with these other Early Precambrian plutonic rocks of the Canadian Shield illustrates that they are characterized by similar Pb concentrations. The average Pb content of the Aulneau batholith samples is generally lower than the Pb values reported in

Table 2. The low Pb concentration of the Aulneau batholith in comparison with the other values reported in Table 2 is attributed to the lower K_2O content of the Aulneau batholith in comparison to the K_2O contents of the other examples listed in Table 2.

Nickel

Based on the ionic radii of Ni^{2+} (0.69 A), Mg^{2+} (0.66 A) and Fe^{2+} (0.75 A), and their respective oxide melting points (NiO, 1990° C; MgO, 2800° C; FeO, 1420° C), the sequence of entrance of these elements into crystal lattices should be Mg, Ni and Fe. Ringwood (1955) suggested that Ni enters early Fe positions rather than Mg positions because of the relationship between their respective electronegativities (Ni^{2+}, 1.8; Mg^{2+}, 1.2; Fe^{2+}, 1.6).

In the Aulneau batholith Ni shows its greatest correlation with MgO ($r = 0.476$). The MgO and Ni relationship is illustrated in Figure 20.

The average Ni content of the Aulneau batholith is generally similar to the values reported for other granitic rocks in Table 2.

Copper

The similarity in size between Cu^{+} ions (0.96 A) and Na^{+} ions (0.97 A), and Cu^{2+} ions (0.72 A) and Fe^{2+} ions (0.75 A) suggests that, according to Goldschmidt's rules, copper should be concentrated in early forming phases of crystallization of a basaltic magma (Taylor, 1965). It has been shown however that copper is concentrated in residual magmas (Wager and Mitchell, 1951).

The magmatic behaviour of copper was explained by Ringwood (1955) as due to the relative weakness of the Cu^{+}-O and Cu^{2+}-O bonds

Table 2. Comparison of the Aulneau batholith chemistry with other granitic rocks.

	1.	2.	3.	4.	5.
SiO_2	70.8	71.6	67.8	67.2	68.4
Al_2O_3	15.9	15.7	16.6	15.5	15.3
FeO	1.8	1.8	3.2	3.8	2.7
CaO	2.6	2.3	3.3	3.5	3.2
MgO	0.8	0.7	2.1	1.6	1.2
Na_2O	5.4	5.2	4.8	3.8	3.4
K_2O	1.6	2.5	2.9	3.0	3.6
TiO_2	0.3	0.3	0.3	0.6	0.4
P_2O_5	0.1	-	0.1	0.2	0.1
MnO	0.1*	0.1*	0.1	0.1	0.1
Li	33	-	-	24	-
Pb	13	13	10	15	20
Ni	10	7	11	15	10
Cu	12	5	4	30	20
Co	6	4	4	7	10
Zn	48	31	11	60	-
Rb	43	-	-	110	118

1. Aulneau batholith, average of 17 trondhjemites and 26 granodiorites.
2. Average of 308 Early Precambrian grandiorites. (Vollrath, 1964)
3. Early Precambrian Opemisca granodiorites. (Wolhuter, 1971)
4. High calcium granitic rocks. (Turekian and Wedepohl, 1961)
5. Average of 193 plutonic rocks from the Sierra Nevada batholith. (Dodge, 1972).

* Less than

in comparison with the Na-O and Fe-O bonds. The weakness of the Cu-O bonds was attributed to the electronegativity differences between Cu^{+} (1.8) and Na^{+} (0.9), and Cu^{2+} (2.0) and Fe^{2+} (1.65).

The relationship between Cu and FeO in the Aulneau batholith is shown in Figure 20. The correlation coefficient for the Cu and FeO relationship is very low (r = 0.289).

The average Cu content of the Aulneau batholith is 12 parts per million. Comparison of the Aulneau batholith with other granitic rocks indicates that the Aulneau batholith has a Cu content higher than other Early Precambrian plutons and a lower Cu content than granitic rocks characterized by higher FeO contents (Table 2).

Cobalt

The ionic radius of Co^{2+} (0.72 A) is intermediate between the ionic radii of Mg^{2+} (0.66 A) and Fe^{2+} (0.75 A) (Taylor, 1965).

The effective ionic radius of Co^{2+} is somewhat less than the accepted value and therefore is rather close to that of Mg^{2+} and as a result tends to show a greater affinity for Mg^{2+} than for Fe^{2+} (Mason, 1966, p. 136).

In a study of the geochemistry of cobalt Carr and Turekian (1961) suggested that in granitic rocks Co^{2+} is strongly coherent with Mg^{2+}.

Linear correlation of Co and MgO is low (r = 0.350). The relationship between Co and MgO is shown in Figure 20.

The average Co concentration of the Aulneau batholith is 6 parts per million and is generally similar to the average Co concentrations reported for other granitic rocks in Table 2.

Zinc

In accordance with Goldschmidt's rules, the similarity between the ionic radii of Zn^{2+} (0.74 A) and Fe^{2+} (0.75 A) suggests that Zn^{2+} should be camouflaged in Fe^{2+} positions. Zn-O bonds are more covalent than Fe-O bonds and therefore Zn^{2+} will enter late Fe^{2+} positions, as a result the Zn^{2+}/ Fe^{2+} ratio will tend to increase during fractionation in silicate melts (Taylor, 1965).

Figure 21 illustrates the relationship between Zn and FeO. The correlation coefficient for the relationship between Zn and FeO is moderately high ($r = 0.610$).

The average Zn content of the Aulneau batholith is 48 parts per million. In comparison with other Early Precambrian granitic rocks the Aulneau batholith has a significantly higher Zn concentration (Table 2). In comparison with high calcium granitic rocks (Table 2) the Aulneau batholith has a similar Zn content.

Rubidium

The geochemical behaviour of rubidium and potassium are closely linked because of the similarity between their ionic radii (Rb^+, 1.44 A; K^+, 1.33 A), electronegativities (Rb^+, 0.8; K^+, 0.8) and ionization potentials (Rb^+, 4.18; K^+, 4.34). Rubidium tends to be slightly concentrated relative to potassium under conditions of extreme fractionation where size differences become significant (Taylor, 1965).

The relationship between Rb and K_2O is shown in Figure 21. The correlation coefficient between Rb and K_2O is moderately high ($r = 0.512$).

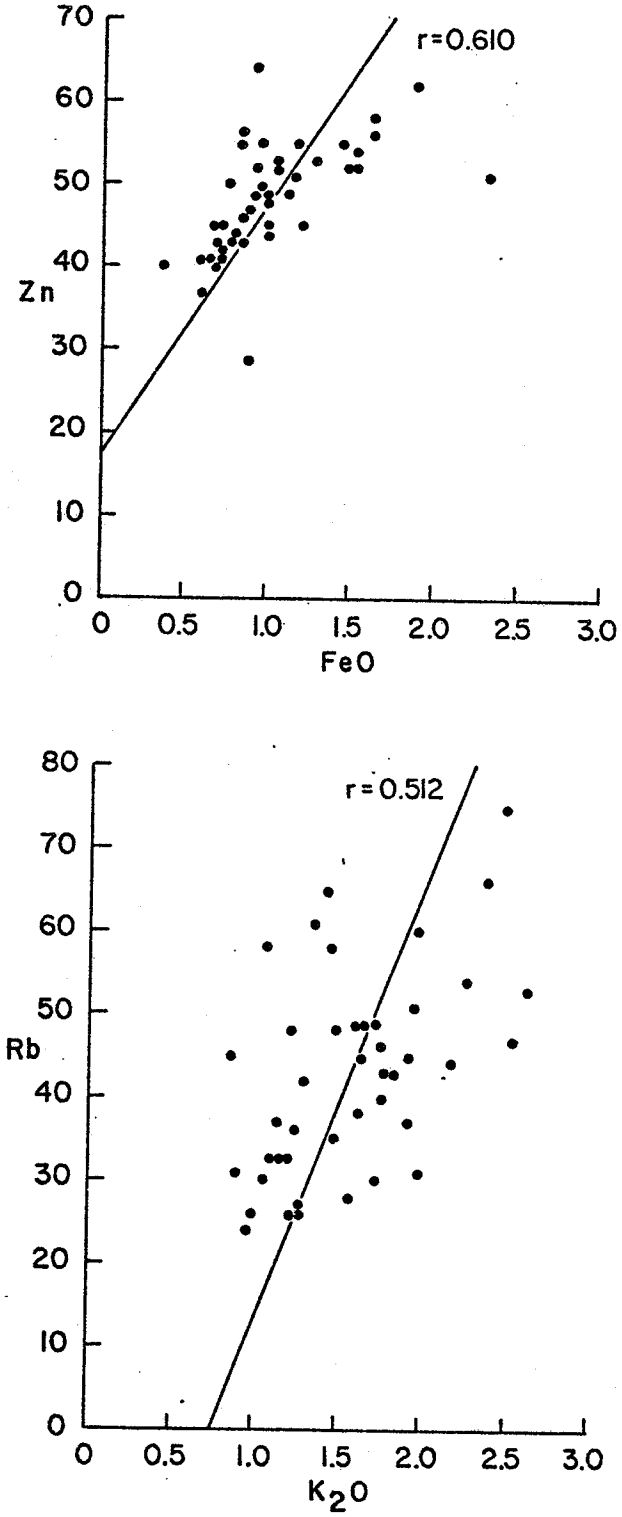

Figure 21. Zn-FeO and Rb-K_2O scatter diagram.

The average Rb content of the Aulneau batholith is 43 parts per million. Comparison of the Aulneau batholith with other granitic rocks listed in Table 2 illustrates that the Aulneau batholith has a significantly lower Rb concentration. When considered in light of the higher K_2O contents of the other granitic rocks listed in Table 2 the low Rb concentration of the Aulneau batholith loses its significance.

Shaw (1968), in a review of K-Rb fractionation trends as determined by covariance analysis determined that the main pattern of K/Rb variation is that shown by a variety of continental and oceanic rock types. The main trend is based on a linear trend on a log-log plot and is described by the equation log (ppm Rb) = 1.115 log (percent K) + 1.597.

The average K/Rb ratios of the early, middle and late intrusive phases of the Aulneau batholith are 268, 265 and 328 respectively, the average K/Rb ratio of the Aulneau batholith is 305. Comparison of the Aulneau batholith samples with Shaws' main trend (Figure 22) illustrates that the Aulneau batholith samples show a trend of increasing K/Rb ratios whereas the K/Rb ratios of the main trend decrease with increasing absolute K and Rb concentrations.

This study illustrates that the concentrations of trace elements investigated are generally similar to those reported for other granitic rocks of similar major element chemistry. The generally low correlation between trace elements and major elements is due possibly to the internal complexity of the phases within the batholith.

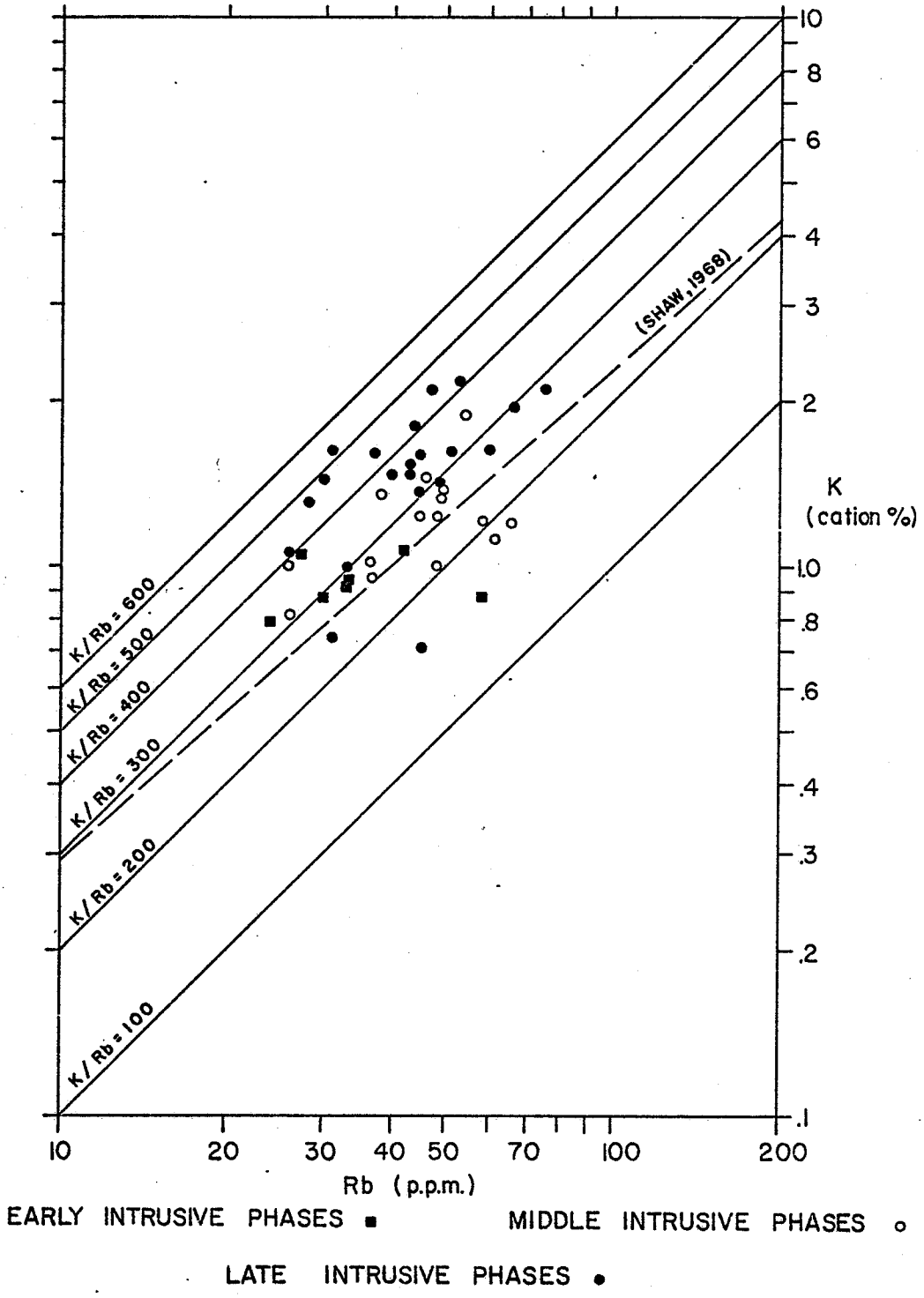

Figure 22. Log Rb - Log K_2O scatter diagram.

ORIGIN OF THE AULNEAU BATHOLITH

The origin of the Aulneau batholith may be considered in light of the four main theories for the origin of granitic rocks; solid-state replacement or granitization, anatexis of quartzose-feldspathic material during high grade regional metamorphism, fractional crystallization of a basaltic magma, and partial melting of amphibolite or eclogite.

Origin of the Aulneau batholith by solid-state replacement is not consistent with the magmatic features of the batholith. Field evidence for magmatic emplacement at the present crustal level includes; generally sharp intrusive contacts between the batholith and the metavolcanic country rock, displacement of the country rock by the batholith, contact metamorphism of the metavolcanic country rock by the batholith, complex intrusive pattern within the batholith as evidenced by contact relationships and distribution of the individual phases. Petrographic evidence for a magmatic origin include; complexly zoned and twinned plagioclase crystals, well developed granophyric textures and the absence of metamorphic minerals indicative of granitization such as garnet or sillimanite.

Origin of the Aulneau batholith by the anatexis of previously existing quartzose-feldspathic material during regional high grade metamorphism is not considered to be a viable mechanism for the generation of the Aulneau batholith because it can not account for the

gabbroic and dioritic phases of the batholith. In addition there is no stratigraphic evidence to suggest that there was a previously existing quartzose-feldspathic material which could act as a parental material.

The calc-alkaline character of the Aulneau batholith reduces the problem of the origin of the batholith to that of the origin of the calc-alkaline igneous rock suite. Fractional crystallization of a basaltic magma and partial melting of amphibolite or eclogite have been investigated as possible mechanisms for the origin of calc-alkaline igneous rocks by Green and Ringwood (1968).

The fractional crystallization of a hydrous magma of basaltic composition at 30 to 40 kilometers depth can produce magmas of the calc-alkaline series (Green and Ringwood, 1968). High degrees of fractional crystallization produces a dacitic or rhyodacitic composition with high K/Na ratios. The low K_2O/Na_2O ratios reported in this study suggest that the Aulneau batholith magmas were not produced by the fractional crystallization of a hydrous basaltic magma.

Green and Ringwood (1968) proposed that partial melting of amphibolite at 30 to 40 kilometers depth under wet conditions ($P_{H2O}<P_{Load}$) could produce calc-alkaline magmas. Under these conditions plagioclase dominates as the melting phase and the K/Na ratios of the magmas produced would decrease with increasing degrees of partial melting. Magmas more acid than andesite would be characterized by a sharp increase in the K_2O/Na_2O ratio. The low K_2O/Na_2O ratios and lack of evidence of a sharp increase in them suggests that the Aulneau batholith did not originate by the partial melting of amphibolite.

Green and Ringwood (1968) suggested that calc-alkaline magmas could be produced by the partial melting of quartz eclogite at depths ranging from 100 to 150 kilometers. Under these conditions calc-alkaline andesitic magma could be produced, magmas more acid than andesite could only be derived by the fractionation of the andesitic magmas in shallow magma chambers (30 to 40 kilometers depth). Under wet conditions ($P_{H2O} < P_{Load}$) at 27 to 36 kilobars, magmas of dacitic or granodioritic composition with K_2O/Na_2O ratios less than unity could be produced. The low K_2O/Na_2O ratios of the Aulneau batholith suggest that this process may have been the mechanism by which the parent magmas were generated.

REFERENCES

Ahrens, L.H.
1966: Element Distributions in Specific Igneous Rocks - VIII; Geochim. et Cosmochim. Acta, Vol. 30, pp. 109 - 122.

Ayres, L.D., Lumbers, S.B., Milne, V.G. and Robeson, D.W.
1970: Ontario Geological Map West Central Sheet; Ontario Dept. Mines and Northern Affairs, Map No. 2199.

Bateman, P.C., Clark, L.D., Huber, N.K., Moore, J.G. and Rinehart, C.D.
1963: The Sierra Nevada Batholith - A Synthesis of Recent Work Across the Central Part; United States Geological Survey, Professional Paper 414 - D, 46 pp.

Brisbin, W.C.
1974: Aulneau Batholith Project, Gravity Studies; Centre for Precambrian Studies Annual Report, Part 2, pp. 185 - 190.

Burns, R.G. and Fyfe, W.S.
1967: Trace Element Distribution Rules and their Significance; Chem. Geol., Vol. 2, pp. 89 - 104.

Carmichael, I.S.E., Turner, F.J. and Verhoogen, J.
1974: Igneous Petrology; McGraw-Hill Inc., New York, 739 pp.

Carr, M.H. and Turekian, K.K.
1961: The Geochemistry of Cobalt; Geochim. et Cosmochim. Acta, Vol. 23, pp. 9 - 60.

Davies, J.C. and Pryslak, A.P.
1965: Lake of the Woods Sheet; Ontario Dept. of Mines, Preliminary Geological Map No. P. 281.

Dodge, F.C.W.
1972: Trace Element Contents of Some Plutonic Rocks of the Sierra Nevada Batholith; United States Geological Survey, Bulletin 1314 - F, 13 pp.

Fraser, N.H.C.
1943: Geology of the Whitefish Bay Area, Lake of the Woods; Ontario Dept. of Mines, Vol. III, Part IV, 19 pp.

Goldschmidt, V.M.
1937: The Principles of Distribution of Chemical Elements in Rocks and Minerals; J. Chem. Soc., 1937; pp. 655 - 672.

Goodwin, A.M.
1965: Preliminary Report on Volcanism and Mineralization in the Lake of the Woods - Manitou Lake - Wabigoon Region of Northwestern Ontario; Ontario Dept. of Mines, Preliminary Report P. R. 1965 - 2, 63 pp.

Green, T.H. and Ringwood, A.E.
1968: Genesis of the Calc-Alkaline Igneous Rock Suite; Contr. Mineral. and Petrol., Vol. 18, pp. 105 - 162.

Hall, D.H., Green, A.G. and Stephenson, O.G.
1974: Seismic and Magnetic Research; Centre for Precambrian Studies Annual Report, Part 2, pp. 3 - 28.

Horstman, E.L.
1957: The Distribution of Lithium, Rubidium and Caesium in Igneous and Sedimentary Rocks; Geochim. et Cosmochim. Acta, Vol. 12, pp. 202 - 222.

Irvine, T.N. and Baragar, W.R.A.
1971: A Guide to the Chemical Classification of the Common Volcanic Rocks; Can. J. Earth Sci., Vol. 8, pp. 523 - 548.

Larsen, E.S.
1938: Some new Variation Diagrams for Groups of Igneous Rocks; Jour. Geol., Vol. 46, pp. 505 - 520.

Lawson, A.C.
1885: Report on the Geology of the Lake of the Woods Region; Geol. Surv. Can., Vol. I, Part CC, pp. 1 - 151.

Lilliefors, H.W.
1967: On the Kolmogorov-Smirnov Test for Normality with Mean and Variance Unknown; Jour. American Statistical Assoc., Vol. 62, pp. 399 - 402.

Mason, B.
1966: Principles of Geochemistry; John Wiley and Sons, Inc., New York, 329 pp.

Mueller, R.F.
1969: Hydration, Oxidation and the Origin of the Calc-Alkali Series; National Aeronautics and Space Administration, NASA TN D-5400, 29 pp.

Nockolds, S.R.
1966: The Behaviour of some Elements During Fractional Crystallization of Magma; Geochim. et Cosmochim. Acta, Vol. 30, pp. 267 - 278.

Nockolds, S.R. and Allen, R.
1953: The Geochemistry of some Igneous Rock Series; Geochim. et Cosmochim. Acta, Vol. 4, pp. 105 - 142.

Ringwood, A.E.
1955: The Principles Governing Trace Element Distribution During Magmatic Crystallization; Geochim. et Cosmochim. Acta, Vol. 7, pp. 189 - 202.

Shaw, D.M.
1968: A Review of K-Rb Fractionation Trends by Covariance Analysis; Geochim. et Cosmochim. Acta, Vol. 32, pp. 573 - 601.

Taylor, S.R.
1965: The Application of Trace Element Data to Problems in Petrology; Phys. Chem. Earth, Vol. 6, pp. 133 - 214.

Thomson, J.E.
1936: Geology of the North Central Part of the Lake of the Woods; Ontario Dept. of Mines, Vol. XLV, Part III, pp. 1 - 43, 1936.

Turekian, K.K. and Wedepohl, K.H.
1961: Distribution of the Elements in Some Major Units of the Earth's Crust; Geol. Soc. America Bull., Vol. 72, pp. 175 - 192.

Vollrath, J.D.
1964: A Geochemical Study of Four Precambrian Granites in Northwestern Ontario; Carlton Univ., Unpub. M.Sc. Thesis, 181 pp.

Wager, L.R. and Mitchell, R.L.
1951: The Distribution of Trace Elements During Strong Fractionation of Basic Magma; Geochim. et Cosmochim. Acta, Vol. 1, pp. 129 - 208.

Wilson, H.D.B., Brisbin, W.C., McRitchie, W.D. and Davies, J.C.
1972: Archean Geology and Metallogenesis of the Western Part of the Canadian Shield; Guidebook for Excursions A33 and C33, XXIV International Geological Congress, Montreal, 63 pp.

Wolhuter, L.E.
1971: The Opemisca Pluton; Quebec Dept. of Natural Resources, Special Paper No. 6, 118 pp.

Ziehlke, D.V.

1972: Report on Preliminary Geological Investigations on the Aulneau Dome, Lake of the Woods Area; Centre for Precambrian Studies, Unpublished report to National Research Council, 31 pp.

1973: Aulneau Batholith Project, Geological Investigations, Progress Report; Centre for Precambrian Studies Annual Report, Appendix III, pp. 60 - 73.

1974: Aulneau Batholith Project, Geology and Petrology; Centre for Precambrian Studies Annual Report, pp. 150 - 184.

APPENDIX 1

Analytical methods, precision and accuracy.

SUMMARY OF METHODS USED IN THE ANALYTICAL LABORATORY

DEPT. OF EARTH SCIENCES- UNIVERSITY OF MANITOBA

Element	Method
Si Al Fe (Total) Mg Ca K Ti Mn	X-ray fluorescence Spectrometry: Weighted sample plus $Li_2B_4O_7$ plus La_2O_3 heated in graphite crucible at about 1100°C for 1/2 hour. Resulting glass bead with H_3BO_3 (Total weight = 2.1000 grams) ground to -200 mesh and then compressed to 50,000 p.s.i. Elements then simultaneously analyzed on multi channel ARL X-ray Spectrometer.
Na_2O, MgO (Low) Cu,Co,Ni,Pb, Cs,Zn,Li,Rb	Atomic Absorption Spectrophotometry: Rock dissolved with HF, H_2SO_4, HNO_3 in platinum crucibles - Perkin Elmer 303. A.A.S.
P_2O_5	Colorimetry: solution as for Na_2O above. The absorption at 430 mμ of molybdivanadophosphoric acid complex - Unicam sp 500 spectrophotometer.
FeO	Rock decomposed with HF and 1:4 H_2SO_4, solution titrated with $K_2Cr_2O_7$ using sodium diphenylamine sulfonate as indicator.
Sn	Fusion of sample with NH_4I at 650°C. SnI dissolved in 25% HCl. A.A.S.
H_2O Total	Determined by heating sample in a stream of dry oxygen in an induction furnace (Temp. 1100°C). H_2O collected on Anhydrone and weighed.
S	Determined by heating samples in an induction furnace with oxygen flowing through combustion chamber. SO_2 evolved is then titrated. Leco Induction furnace and automatic titrator.
CO_2	Sample decomposed by HCl and heat. CO_2 evolved passed through drying train and collected on Ascarite.
CO_2 (low S samples)	Determined simultaneously with H_2O (Total). CO_2 collected on Ascarite.

PRECISION AND ACCURACY OF MAJOR ELEMENTS

Constituent	Concentration %	Instrument Precision	Accuracy of Replicates
			STD. DEV.
SiO_2	59.60	.12	.20
Al_2O_3	9.34	.05	.13
Fe_2O_3 (Total)	10.08	.017	.03
MgO	4.04	.04	.10
CaO	10.22	.02	.07
K_2O	2.69	.01	.01
MnO	.41	.01	.01
TiO_2	.48	.02	.02
Na_2O	4.20	.01	.05
H_2O (Total)	1.60	.03	.06
CO_2	1.15	.05	.12
P_2O_5	0.20	.01	.01
FeO	10.92	--	0.04
S	0.185	0.003	0.005

PRECISION AND ACCURACY OF TRACE ELEMENTS

Constituent	Concentration	Instrument Precision	Accuracy of Replicates
		STD. DEV.	
Cs	820 ppm	5.0	13.0
Co	53 ppm	1.0	2.0
Cu	40 ppm	1.0	2.0
Li	10 ppm	.04	.05
Ni	77 ppm	1.0	3.0
Pb	34 ppm	2.0	3.0
Rb	228 ppm	1.0	2.0
Zn	108 ppm	1.0	2.0

APPENDIX 2

Chemical Analyses

Major elements in weight percent

Trace elements in parts per million

- Not detected

N.D. Not determined

Early Intrusive Phases

Phase No.	1	1	1	1	1	1	1
Sample No.	Z 81	Z 90	Z 91	Z 97	Z 98	Z 112	Z 116
SiO_2	71.25	69.45	71.50	68.10	70.55	73.50	67.70
Al_2O_3	15.75	15.78	16.02	15.82	15.80	14.88	15.56
Fe_2O_3	0.57	1.04	0.32	1.16	0.65	0.50	0.83
FeO	1.16	1.64	1.00	1.88	1.28	1.04	2.32
CaO	2.50	3.14	2.61	4.15	2.82	2.44	4.52
MgO	0.73	1.06	0.68	1.24	0.88	0.59	1.49
Na_2O	5.67	5.53	5.62	4.67	5.73	5.22	4.79
K_2O	1.26	1.15	1.29	1.11	1.06	0.96	1.06
TiO_2	0.28	0.26	0.17	0.41	0.29	0.18	0.43
P_2O_5	0.10	0.12	0.09	0.14	0.15	0.08	0.15
MnO	0.02	0.05	0.02	0.05	0.02	0.03	0.05
H_2O	0.18	0.72	0.45	0.63	0.58	0.43	0.65
S	0.01	0.00	0.01	0.01	0.01	0.01	0.01
CO_2	0.07	0.11	0.06	0.08	0.01	0.09	0.08
TOTAL	99.55	100.05	99.84	99.45	99.92	99.95	99.64
Li	23	39	30	35	20	29	53
Pb	17	3	9	5	5	6	23
Ni	6	1	9	14	7	14	21
Cu	15	10	8	19	22	7	14
Co	2	14	7	6	9	1	12
Zn	51	56	49	62	53	53	51
Rb	27	33	42	33	30	24	58
Sn	21	-	-	-	-	-	-
Cs	-	-	-	12	-	-	-

Middle Intrusive Phases

Phase No.	6	6	3	14	13	13	14
Sample No.	Z 12	Z 14	Z 51	Z 85	Z 88	Z 96	Z 100
SiO_2	68.75	70.25	72.65	73.05	69.90	69.80	72.80
Al_2O_3	16.02	15.98	15.75	15.42	16.08	16.17	15.26
Fe_2O_3	1.15	0.86	0.39	0.36	0.74	0.26	0.67
FeO	0.96	1.00	0.60	0.80	1.04	1.00	0.80
CaO	2.85	2.55	2.12	1.97	2.68	2.90	2.36
MgO	1.07	0.73	0.46	0.42	0.86	0.68	0.49
Na_2O	5.04	5.24	4.97	5.08	5.53	5.86	5.52
K_2O	1.42	1.45	1.65	2.27	1.62	1.48	1.13
TiO_2	0.34	0.29	0.23	0.18	0.26	0.26	0.22
P_2O_5	0.10	0.11	0.07	0.07	0.12	0.10	0.09
MnO	0.03	0.02	0.03	0.02	0.03	0.02	0.03
H_2O	0.86	0.49	0.49	0.43	0.72	0.46	0.54
S	0.00	0.00	0.00	0.00	0.00	0.01	0.00
CO_2	0.18	0.06	0.08	0.01	0.06	0.12	0.12
TOTAL	98.76	99.03	99.49	100.08	99.64	99.12	100.03
Li	58	37	35	18	37	35	43
Pb	10	9	11	52	30	7	19
Ni	13	2	7	6	13	11	10
Cu	11	10	3	17	11	10	13
Co	5	6	2	4	8	6	7
Zn	55	48	37	29	53	45	44
Rb	65	58	49	54	38	45	37
Sn	N.D.	N.D.	2	2	-	-	12
Cs	N.D.	N.D.	-	-	-	-	-

Middle Intrusive Phases

Phase No.	3	7	6	8	8	8	7	7
Sample No.	Z 104	Z 108	Z 399	Z 472	Z 473	Z 479	Z 2364	Z 2366
SiO_2	69.55	69.25	68.35	71.25	68.90	70.40	69.45	68.25
Al_2O_3	15.76	16.13	16.12	14.14	15.20	15.62	15.80	15.96
Fe_2O_3	0.79	1.38	0.87	1.59	1.35	1.07	1.30	1.70
FeO	1.52	1.48	1.12	0.92	1.44	0.88	0.92	0.84
CaO	3.09	3.15	2.90	2.85	3.04	2.59	2.62	2.88
MgO	1.04	1.21	0.91	0.94	1.23	0.67	0.93	1.16
Na_2O	4.98	5.08	5.24	4.88	5.32	5.68	5.16	5.32
K_2O	1.75	1.23	1.35	0.99	1.21	1.22	1.62	1.49
TiO_2	0.31	0.24	0.32	0.35	0.39	0.28	0.31	0.32
P_2O_5	0.13	0.15	0.11	0.12	0.13	0.09	0.12	0.13
MnO	0.05	0.04	0.03	0.03	0.04	0.03	0.04	0.04
H_2O	0.70	0.72	0.55	0.85	0.53	0.56	0.55	0.73
S	0.00	0.00	0.00	0.00	0.00	0.01	0.00	0.00
CO_2	0.50	0.17	0.21	0.10	0.03	0.02	0.04	0.00
TOTAL	100.17	100.23	98.08	99.01	98.81	99.12	98.99	98.82
Li	38	25	44	20	35	25	41	31
Pb	19	2	6	7	7	7	2	2
Ni	16	29	8	2	8	4	13	13
Cu	20	11	23	21	19	29	14	24
Co	3	5	7	6	11	10	12	11
Zn	52	52	49	49	55	47	52	55
Rb	46	36	61	26	48	26	49	48
Sn	7	2	N.D.	N.D.	N.D.	N.D.	N.D.	N.D.
Cs	-	-	N.D.	N.D.	N.D.	N.D.	N.D.	N.D.

Late Intrusive Phases

Phase No.	18	15	15	17	17	18	18
Sample No.	Z 9	Z 13	Z 15	Z 19	Z 22	Z 24	Z 60
SiO_2	67.85	71.10	71.10	70.40	69.35	70.50	72.65
Al_2O_3	16.65	16.55	16.35	16.54	17.09	16.20	15.62
Fe_2O_3	0.72	0.49	0.33	0.75	0.94	1.80	0.47
FeO	1.52	0.72	0.72	0.96	0.92	0.60	0.72
CaO	2.68	2.50	2.00	2.50	3.21	2.05	2.20
MgO	1.28	0.54	0.41	0.72	1.06	0.60	0.47
Na_2O	5.92	6.15	5.82	5.92	6.90	5.53	5.20
K_2O	1.77	1.28	1.64	1.19	0.89	1.78	1.93
TiO_2	0.31	0.21	0.23	0.24	0.27	0.22	0.19
P_2O_5	0.22	0.09	0.08	0.08	0.11	0.08	0.07
MnO	0.06	0.03	0.02	0.03	0.05	0.03	0.02
H_2O	0.69	0.46	0.37	1.46	0.66	0.72	0.59
S	0.00	0.00	0.00	0.01	0.00	0.00	0.00
CO_2	0.08	0.04	0.03	0.09	0.10	0.15	0.04
TOTAL	99.25	100.16	99.10	100.89	101.55	100.26	100.17
Li	15	30	36	37	41	32	31
Pb	24	14	20	9	14	28	21
Ni	9	-	1	-	9	8	17
Cu	17	3	4	2	6	17	5
Co	2	-	9	-	8	-	8
Zn	54	45	41	50	64	41	42
Rb	40	26	45	33	31	43	37
Sn	-	-	-	-	-	-	2
Cs	-	-	-	-	-	-	-

Late Intrusive Phases

Phase No.	18	17	17	17	17	17	17
Sample No.	Z 63	Z 64	Z 66	Z 70	Z 72	Z 73	Z 83
SiO_2	64.65	72.55	71.50	71.65	72.45	72.60	70.90
Al_2O_3	16.62	15.36	16.09	15.44	14.99	15.56	16.06
Fe_2O_3	1.62	0.79	0.34	0.70	0.61	0.46	0.42
FeO	1.64	0.68	0.84	1.00	0.68	0.64	0.84
CaO	3.08	2.22	2.12	2.44	2.04	2.21	2.59
MgO	1.54	0.57	0.53	0.61	0.48	0.47	0.43
Na_2O	6.08	5.05	5.00	5.20	4.99	5.08	5.56
K_2O	1.74	2.16	2.61	1.98	2.53	1.91	1.57
TiO_2	0.36	0.19	0.21	0.24	0.21	0.18	0.24
P_2O_5	0.27	0.09	0.08	0.10	0.09	0.07	0.09
MnO	0.05	0.03	0.03	0.02	0.02	0.03	0.02
H_2O	1.01	0.54	0.45	0.59	0.57	0.50	0.93
S	0.00	0.01	0.00	0.01	0.00	0.01	0.00
CO_2	0.07	0.07	0.09	0.07	0.12	0.05	0.01
TOTAL	98.73	100.31	99.89	100.05	99.78	99.77	99.75
Li	21	40	40	28	26	48	21
Pb	31	33	2	2	19	7	12
Ni	19	8	15	4	10	7	-
Cu	5	10	10	2	9	2	5
Co	13	8	12	13	4	5	-
Zn	58	45	43	44	40	41	56
Rb	30	44	53	31	47	45	28
Sn	-	-	7	5	7	14	-
Cs	-	-	-	-	-	-	-

Late Intrusive Phases

Phase No.	16	15	17	16	16	18	18
Sample No.	Z 89	Z 110	Z 120	Z 145	Z 150	Z 194	Z 2190
SiO_2	71.90	71.60	70.95	71.95	73.10	71.05	66.70
Al_2O_3	15.89	15.42	14.78	15.64	15.42	16.13	16.47
Fe_2O_3	0.27	0.57	1.12	0.74	0.56	0.69	1.44
FeO	0.84	0.76	1.20	0.76	0.40	0.68	1.16
CaO	1.85	2.60	2.84	2.08	1.66	2.05	2.30
MgO	0.42	0.64	1.07	0.58	0.31	0.52	1.14
Na_2O	5.30	5.29	4.91	6.12	5.52	5.52	5.68
K_2O	2.49	1.71	1.83	0.85	1.97	1.95	2.37
TiO_2	0.19	0.22	0.29	0.22	0.17	0.24	0.33
P_2O_5	0.09	0.09	0.12	0.07	0.05	0.09	0.20
MnO	0.02	0.03	0.04	0.02	0.02	0.02	0.05
H_2O	0.40	0.43	0.68	0.45	0.35	0.33	0.58
S	0.00	0.00	0.01	0.01	0.00	0.00	0.00
CO_2	0.07	0.70	0.08	0.05	0.01	0.03	0.07
TOTAL	99.73	100.06	99.92	100.13	99.85	99.82	99.63
Li	30	27	28	44	33	26	41
Pb	10	14	19	1	7	13	16
Ni	4	3	38	4	8	8	8
Cu	10	11	8	14	7	8	14
Co	3	-	3	10	5	4	6
Zn	46	43	45	50	37	43	55
Rb	75	49	43	45	60	51	66
Sn	-	10	2	N.D.	N.D.	N.D.	N.D.
Cs	-	-	-	N.D.	N.D.	N.D.	N.D.

APPENDIX 3

Modal Mineralogy

Early Intrusive Phases

Phase No.	1	1	1	1	1	1	1
Sample No.	Z 81	Z 90	Z 91	Z 97	Z 98	Z 112	Z 116
Quartz	28.6	28.3	27.5	29.6	23.0	32.2	23.0
Plagioclase	55.4	58.7	61.8	60.4	63.5	60.8	59.8
K Feldspar	6.3	2.1	3.7	2.6	4.5	4.1	0.0
Biotite	6.6	7.9	5.3	5.0	5.8	1.9	9.3
Hornblende	0.0	0.0	0.0	0.9	0.3	0.0	5.6
Chlorite	0.0	0.2	0.0	0.0	0.2	0.1	0.1
Epidote	1.7	1.8	0.9	1.6	1.7	0.5	1.0
Apatite	0.1	0.1	0.1	0.1	0.1	0.1	0.3
Zircon	tr	tr	0.1	0.1	0.1	tr	0.1
Allanite	0.1	0.1	0.1	0.1	0.1	0.0	0.0
Sphene	0.6	0.5	0.3	0.2	0.5	0.0	0.7
Opaque	0.5	0.3	0.2	0.1	0.2	0.3	0.1

Middle Intrusive Phases

Phase No.	6	6	3	14	13	13	14
Sample No.	Z 12	Z 14	Z 51	Z 85	Z 88	Z 96	Z 100
Quartz	28.9	29.8	31.2	25.4	26.8	21.8	32.7
Plagioclase	55.9	53.4	50.6	57.0	56.0	63.4	52.8
K Feldspar	5.2	5.0	12.3	13.7	8.6	7.0	7.9
Biotite	5.0	6.9	4.2	0.8	4.2	6.1	3.5
Hornblende	0.0	0.0	0.0	0.0	0.4	0.0	0.0
Chlorite	0.7	0.0	0.0	0.6	0.4	0.0	0.0
Epidote	3.6	3.8	1.2	1.4	1.8	0.9	1.9
Apatite	0.2	0.1	0.1	0.1	tr	0.1	0.1
Zircon	tr	0.1	tr	0.1	tr	tr	tr
Allanite	0.1	0.3	0.2	0.3	tr	0.2	0.1
Sphene	0.3	0.3	0.1	0.2	0.8	0.2	0.4
Opaque	0.1	0.3	0.1	0.3	0.8	0.1	0.6

Middle Intrusive Phases

Phase No.	3	7	6	8	8	8	7	7
Sample No.	Z 104	Z 108	Z 399	Z 472	Z 473	Z 479	Z 2364	Z 2366
Quartz	30.8	25.8	28.9	25.5	25.1	22.7	21.9	18.2
Plagioclase	48.4	59.5	55.8	58.3	58.9	66.7	54.5	51.6
K Feldspar	8.8	5.0	3.5	1.5	3.4	3.1	4.5	4.5
Biotite	8.4	6.4	5.9	9.1	8.1	4.9	10.3	14.5
Hornblende	0.0	0.4	0.0	0.0	1.3	0.0	1.0	0.3
Chlorite	0.0	0.0	0.2	0.0	0.0	0.7	0.1	0.6
Epidote	2.9	1.8	4.7	4.1	2.0	0.7	5.9	7.0
Apatite	0.1	0.1	0.1	tr	0.1	0.1	0.1	0.1
Zircon	tr	0.1	0.1	tr	0.1	tr	0.1	tr
Allanite	0.1	0.2	0.1	0.0	0.2	0.1	0.1	0.2
Sphene	0.4	0.3	0.4	0.8	0.3	0.7	0.4	1.8
Opaque	0.1	0.4	0.3	0.3	0.3	0.3	1.1	1.0

Late Intrusive Phases

Phase No.	18	15	15	17	17	18	18
Sample No.	Z 9	Z 13	Z 15	Z 19	Z 22	Z 24	Z 60
Quartz	21.3	24.3	27.9	26.5	21.8	27.0	28.5
Plagioclase	42.4	54.2	56.0	56.1	68.1	56.9	49.6
K Feldspar	21.5	14.3	10.6	8.4	0.0	9.0	15.2
Biotite	4.1	3.0	3.5	5.7	5.7	4.9	4.6
Hornblende	8.0	0.7	0.0	0.0	0.0	0.0	0.0
Chlorite	0.0	0.2	0.2	0.0	0.0	0.0	0.0
Epidote	1.0	2.5	1.1	2.4	3.7	1.6	1.4
Apatite	0.2	0.1	tr	0.1	0.1	0.1	0.1
Zircon	tr	tr	tr	tr	0.1	0.1	0.1
Allanite	0.2	0.1	0.1	0.0	0.0	0.1	tr
Sphene	0.9	0.3	0.3	0.4	0.3	0.2	0.2
Opaque	0.1	0.3	0.3	0.4	0.2	0.2	0.3

Late Intrusive Phases

Phase No.	18	17	17	17	17	17	17
Sample No.	Z 63	Z 64	Z 66	Z 70	Z 72	Z 73	Z 83
Quartz	19.0	23.8	26.4	28.4	27.6	29.7	22.4
Plagioclase	47.4	57.0	52.0	49.9	50.6	44.1	63.2
K Feldspar	13.3	14.8	14.4	16.0	16.0	19.1	10.0
Biotite	6.3	2.8	4.3	4.1	3.3	4.3	3.1
Hornblende	6.3	0.0	0.0	0.0	0.0	0.0	0.0
Chlorite	1.0	0.0	0.2	0.0	0.0	0.0	0.0
Epidote	3.4	1.1	2.1	0.7	0.7	2.1	0.7
Apatite	tr	0.0	0.1	tr	tr	0.1	0.1
Zircon	0.1	tr	tr	tr	tr	tr	tr
Allanite	0.1	0.1	tr	0.1	0.0	tr	tr
Sphene	1.9	0.2	0.3	0.6	0.4	0.4	0.3
Opaque	1.2	0.2	0.2	0.2	0.4	0.2	0.2

Late Intrusive Phases

Phase No.	16	15	17	16	16	18	18
Sample No.	Z 89	Z 110	Z 120	Z 145	Z 150	Z 194	Z 2190
Quartz	23.8	24.2	26.9	25.4	25.1	31.5	13.7
Plagioclase	55.0	56.5	50.3	64.6	58.0	56.0	50.5
K Feldspar	14.4	11.6	11.8	0.0	12.6	7.1	22.1
Biotite	3.9	4.7	6.5	6.7	2.8	4.3	3.7
Hornblende	0.0	0.0	0.0	0.2	0.0	0.0	6.7
Chlorite	0.3	0.2	0.3	0.1	0.1	0.1	0.0
Epidote	2.1	1.5	3.5	1.5	1.3	0.6	1.5
Apatite	0.1	0.1	tr	0.1	tr	tr	0.1
Zircon	tr	0.1	0.1	tr	0.0	0.0	tr
Allanite	tr	0.1	0.0	0.0	0.0	tr	0.3
Sphene	0.2	0.6	0.3	0.7	0.0	0.2	0.9
Opaque	0.2	0.4	0.3	0.7	0.1	0.2	0.5

APPENDIX 4

Normative Mineralogy

Early Intrusive Phases

Phase No.	1	1	1	1	1	1	1
Sample No.	Z 81	Z 90	Z 91	Z 97	Z 98	Z 112	Z 116
Quartz	24.92	22.61	25.05	24.61	23.96	30.94	22.30
Albite	50.90	49.71	50.39	42.49	51.42	47.08	43.43
Anorthite	11.31	14.12	11.97	19.19	12.37	11.07	18.01
Orthoclase	7.45	6.81	7.62	6.65	6.27	5.70	6.33
Diopside	0.00	0.00	0.00	0.13	0.00	0.00	1.56
Ferrosilite	1.04	1.53	1.12	1.60	1.16	1.06	2.05
Enstatite	2.02	2.93	1.88	3.40	2.43	1.66	3.37
Magnetite	0.60	1.09	0.33	1.23	0.68	0.53	0.88
Hypersthene	0.00	0.00	0.00	0.06	0.00	0.00	0.95
Ilmenite	0.39	0.36	0.24	0.58	0.40	0.25	0.61
Apatite	0.21	0.25	0.19	0.30	0.31	0.17	0.32
Corundum	1.00	0.30	1.08	0.00	0.75	1.37	0.00
Calcite	0.16	0.25	0.14	0.18	0.23	0.21	0.18
Pyrite	0.00	0.00	0.00	0.00	0.00	0.00	0.00
Hematite	0.00	0.00	0.00	0.00	0.00	0.00	0.00

Middle Intrusive Phases

Phase No.	6	6	3	14	13	13	14
Sample No.	Z 12	Z 14	Z 51	Z 85	Z 88	Z 96	Z 100
Quartz	25.37	26.05	30.26	27.60	22.84	21.23	28.65
Albite	46.03	47.56	44.99	45.65	49.81	52.73	49.64
Anorthite	12.56	11.68	9.64	9.26	12.17	13.01	10.38
Orthoclase	8.54	8.67	9.84	13.44	9.61	8.77	6.69
Diopside	0.00	0.00	0.00	0.00	0.00	0.00	0.00
Ferrosilite	0.26	0.58	0.39	0.77	0.78	1.04	0.51
Enstatite	3.01	2.04	1.28	1.16	2.38	1.88	1.36
Magnetite	1.22	0.91	0.41	0.38	0.78	0.27	0.70
Hypersthene	0.00	0.00	0.00	0.00	0.00	0.00	0.00
Ilmenite	0.48	0.41	0.32	0.25	0.36	0.36	0.31
Apatite	0.21	0.23	0.15	0.15	0.25	0.21	0.19
Corundum	1.85	1.72	2.52	1.33	0.86	0.19	1.27
Calcite	0.42	0.14	0.18	0.02	0.14	0.28	0.28
Pyrite	0.00	0.00	0.00	0.00	0.00	0.00	0.00
Hematite	0.00	0.00	0.00	0.00	0.00	0.00	0.00

Middle Intrusive Phases

Phase No.	3	7	6	8	8	8	7	7
Sample No.	Z 104	Z 108	Z 399	Z 472	Z 473	Z 479	Z 2364	Z 2366
Quartz	27.73	24.84	24.19	30.48	23.47	24.58	24.97	22.61
Albite	44.78	45.72	47.95	44.80	48.44	51.43	46.96	48.44
Anorthite	11.34	13.61	12.58	13.01	14.22	12.24	12.13	13.63
Orthoclase	10.37	7.29	8.14	5.99	7.26	7.28	9.71	8.94
Diopside	0.00	0.00	0.00	0.00	0.01	0.00	0.00	0.00
Ferrosilite	1.45	1.06	0.74	0.00	0.82	0.26	0.15	0.00
Enstatite	2.88	3.35	2.56	2.65	3.44	1.87	2.60	3.25
Magnetite	0.83	1.45	0.93	1.51	1.43	1.13	1.38	1.40
Hypersthene	0.00	0.00	0.00	0.00	0.00	0.00	0.00	0.00
Ilmenite	0.43	0.34	0.45	0.50	0.55	0.39	0.44	0.45
Apatite	0.27	0.32	0.24	0.26	0.28	0.19	0.26	0.28
Corundum	1.67	1.61	1.69	0.42	0.00	0.56	1.30	0.74
Calcite	1.16	0.39	0.49	0.23	0.07	0.05	0.09	0.00
Pyrite	0.00	0.00	0.00	0.00	0.00	0.03	0.00	0.00
Hematite	0.00	0.00	0.00	0.13	0.00	0.00	0.00	0.27

Late Intrusive Phases

Phase No.	18	15	15	17	17	18	18
Sample No.	Z 9	Z 13	Z 15	Z 19	Z 22	Z 24	Z 60
Quartz	17.54	22.35	24.20	23.14	16.23	24.88	27.44
Albite	52.95	54.73	52.41	52.94	60.27	49.63	46.72
Anorthite	11.31	11.46	9.24	11.27	12.68	8.70	10.21
Orthoclase	10.43	7.50	9.73	7.01	5.12	10.53	11.42
Diopside	0.00	0.00	0.00	0.00	1.03	0.00	0.00
Ferrosilite	1.51	0.52	0.60	0.67	0.38	0.00	0.56
Enstatite	3.52	1.48	1.14	1.98	2.33	1.66	1.30
Magnetite	0.75	0.51	0.35	0.78	0.96	1.01	0.49
Hypersthene	0.00	0.00	0.00	0.00	0.17	0.00	0.00
Ilmenite	0.43	0.29	0.32	0.33	0.37	0.31	0.27
Apatite	0.46	0.19	0.17	0.17	0.22	0.17	0.15
Corundum	0.91	0.88	1.78	1.49	0.00	2.17	1.35
Calcite	0.18	0.09	0.07	0.21	0.23	0.34	0.09
Pyrite	0.00	0.00	0.00	0.00	0.00	0.00	0.00
Hematite	0.00	0.00	0.00	0.00	0.00	0.58	0.00

Late Intrusive Phases

Phase No.	18	17	17	17	17	17	17
Sample No.	Z 63	Z 64	Z 66	Z 70	Z 72	Z 73	Z 83
Quartz	13.24	27.41	25.13	25.76	27.04	28.27	24.66
Albite	55.04	45.35	44.93	46.79	45.05	45.82	50.16
Anorthite	13.03	9.99	9.43	11.04	8.82	10.24	11.69
Orthoclase	10.38	12.78	15.45	11.74	15.05	11.35	9.33
Diopside	0.10	0.00	0.00	0.00	0.00	0.00	0.00
Ferrosilite	0.99	0.29	0.82	0.76	0.37	0.47	0.71
Enstatite	4.24	1.57	1.46	1.69	1.33	1.30	1.19
Magnetite	1.71	0.83	0.36	0.73	0.64	0.48	0.44
Hypersthene	0.02	0.00	0.00	0.00	0.00	0.00	0.00
Ilmenite	0.51	0.27	0.29	0.34	0.29	0.25	0.34
Apatite	0.57	0.19	0.17	0.21	0.19	0.15	0.19
Corundum	0.00	1.15	1.73	0.77	0.91	1.54	1.05
Calcite	0.16	0.16	0.21	0.16	0.28	0.12	0.23
Pyrite	0.00	0.00	0.00	0.00	0.00	0.00	0.00
Hematite	0.00	0.00	0.00	0.00	0.00	0.00	0.00

Late Intrusive Phases

Phase No.	16	15	17	16	16	18	18
Sample No.	Z 89	Z 110	Z 120	Z 145	Z 150	Z 194	Z 2190
Quartz	24.94	27.38	26.00	25.86	27.47	24.62	17.29
Albite	47.60	47.37	44.41	54.96	49.69	49.72	51.49
Anorthite	8.15	7.87	12.90	9.55	7.87	9.42	9.76
Orthoclase	14.73	10.09	10.90	5.03	11.68	11.57	14.15
Diopside	0.00	0.00	0.00	0.00	0.00	0.00	0.00
Ferrosilite	0.88	0.52	0.74	0.37	0.02	0.27	0.42
Enstatite	1.16	1.76	2.98	1.60	0.86	1.44	3.18
Magnetite	0.28	0.59	1.18	0.77	0.59	0.72	1.52
Hypersthene	0.00	0.00	0.00	0.00	0.00	0.00	0.00
Ilmenite	0.27	0.31	0.41	0.31	0.24	0.34	0.46
Apatite	0.19	0.19	0.25	0.15	0.11	0.19	0.42
Corundum	1.63	2.15	0.03	1.26	1.46	1.64	1.12
Calcite	0.16	1.62	0.18	0.12	0.03	0.07	0.16
Pyrite	0.00	0.00	0.00	0.03	0.00	0.00	0.00
Hematite	0.00	0.00	0.00	0.00	0.00	0.00	0.00

APPENDIX 5

Age relationships and distribution of the phases within the Aulneau Batholith (after Ziehlke, 1974)

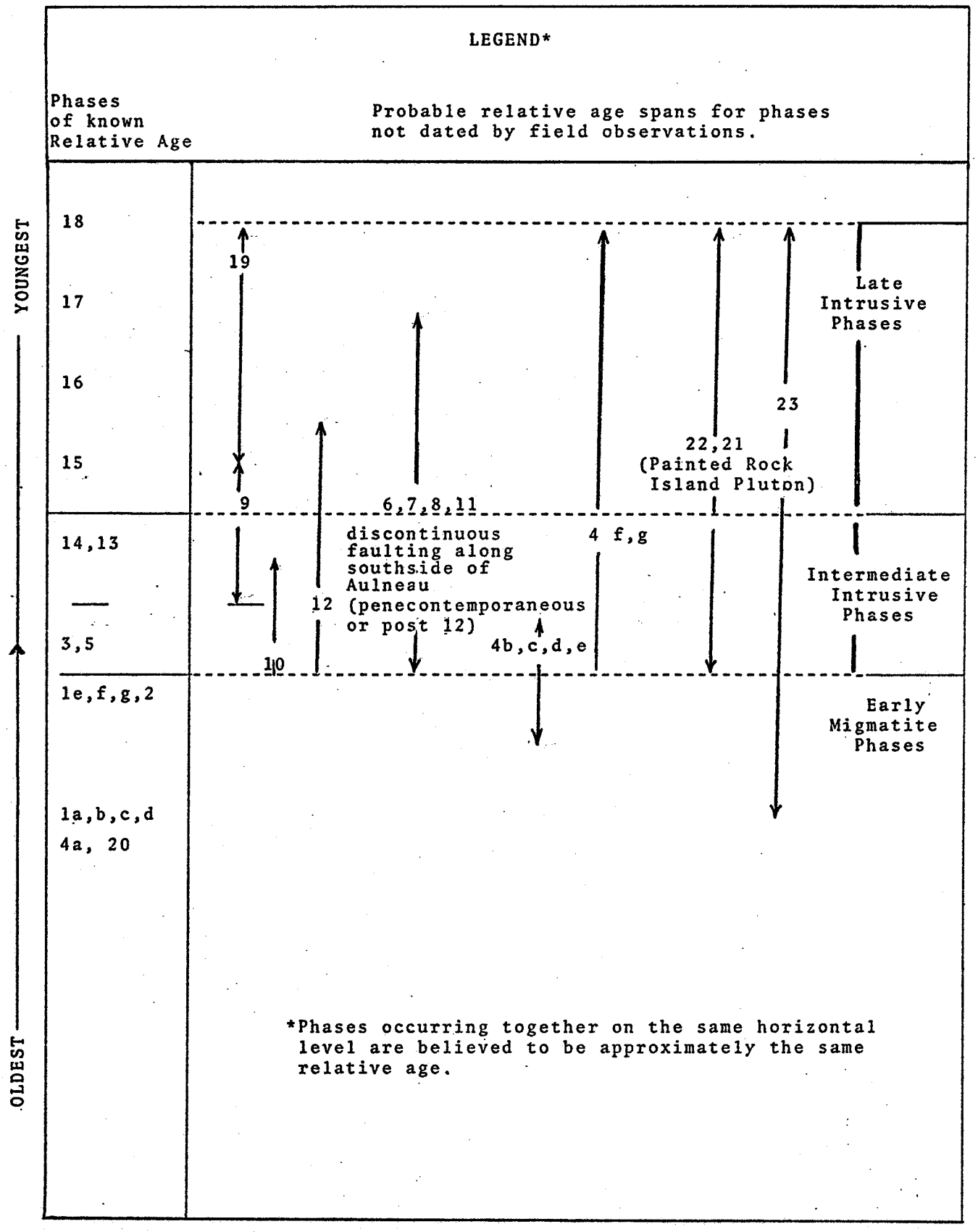
LEGEND*
Phases of known Relative Age
Probable relative age spans for phases not dated by field observations.
YOUNGEST
OLDEST
18
17
16
15
14,13
3,5
1e,f,g,2
1a,b,c,d
4a, 20
19
9
10
12
6,7,8,11
discontinuous faulting along southside of Aulneau (penecontemporaneous or post 12)
4b,c,d,e
4 f,g
22,21 (Painted Rock Island Pluton)
23
Late Intrusive Phases
Intermediate Intrusive Phases
Early Migmatite Phases
*Phases occurring together on the same horizontal level are believed to be approximately the same relative age.

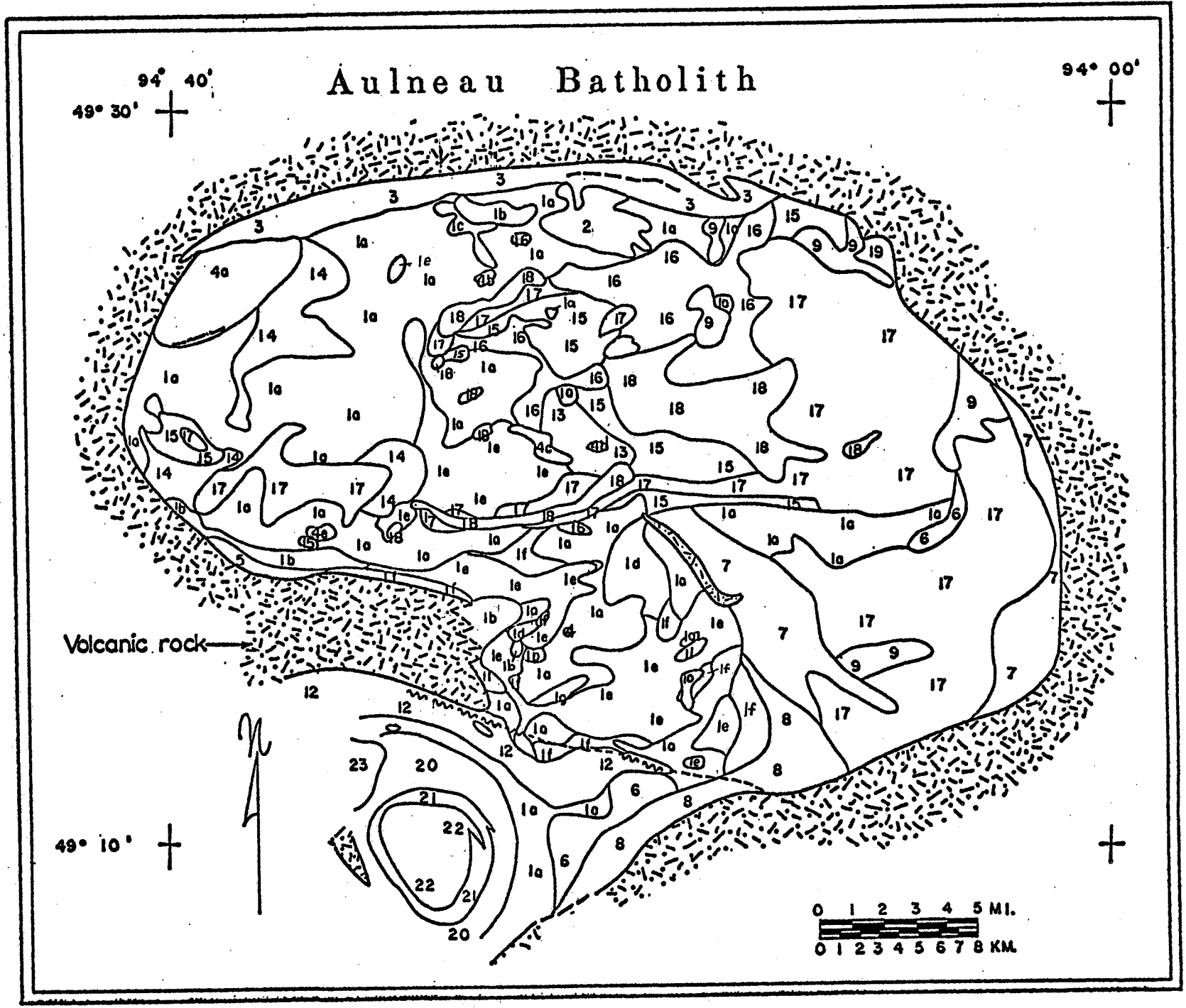
Aulneau Batholith
94° 40'
49° 30'
94° 00'
49° 10'
Volcanic rock
0 1 2 3 4 5 MI.
0 1 2 3 4 5 6 7 8 KM.

APPENDIX 6

Kolmogorov-Smirnov Statistics

ELEMENT	D VALUE WHEN ARITHMETIC VALUES TESTED AS NORMAL	D VALUE WHEN LOGARITHMIC VALUES TESTED AS NORMAL	CRITICAL VALUES OF D AT VARIOUS LEVELS OF SIGNIFICANCE		
			0.20	0.10	0.05
SiO_2	0.098	0.102	0.112	0.123	0.135
Al_2O_3	0.076	0.075	0.112	0.123	0.135
Fe_2O_3	0.136	0.061	0.112	0.123	0.135
FeO	0.178	0.107	0.112	0.123	0.135
CaO	0.107	0.075	0.112	0.123	0.135
MgO	0.153	0.115	0.112	0.123	0.135
Na_2O	0.122	0.109	0.112	0.123	0.135
K_2O	0.109	0.083	0.112	0.123	0.135
TiO_2	0.145	0.108	0.112	0.123	0.135
P_2O_5	0.170	0.152	0.112	0.123	0.135
MnO	0.254	0.222	0.112	0.123	0.135
H_2O	0.144	0.104	0.112	0.123	0.135
S	0.431	0.431	0.112	0.123	0.135
CO_2	0.302	0.416	0.112	0.123	0.135
Li	0.058	0.064	0.112	0.123	0.135
Pb	0.138	0.099	0.112	0.123	0.135
Ni	0.153	0.452	0.112	0.123	0.135
Cu	0.143	0.116	0.112	0.123	0.135
Co	0.079	0.483	0.112	0.123	0.135
Zn	0.083	0.077	0.112	0.123	0.135
Rb	0.100	0.100	0.112	0.123	0.135
Sn	0.382	0.442	0.132	0.145	0.159
Cs	0.538	0.538	0.132	0.145	0.159

APPENDIX 7

Linear Regression Analysis of Major and Trace Elements with Larsen Differentiation Indices

EARLY INTRUSIVE PHASES

ELEMENT	SLOPE	Y INTERCEPT	CORRELATION COEFFICIENT
SiO_2	0.772	56.176	0.956
Al_2O_3	-0.02	16.02	0.02
Fe_2O_3	-0.096	2.479	0.808
FeO	-0.192	4.985	0.985
CaO	-0.325	9.111	0.980
MgO	-0.128	3.293	0.994
Na_2O	0.130	2.941	0.756
K_2O	0.010	0.944	0.228
TiO_2	-0.036	0.946	0.945
P_2O_5			
MnO	-0.005	0.125	0.632
H_2O	-0.050	1.434	0.698
Li	-3.413	95.116	0.779
Pb	-0.871	25.647	0.295
Ni	-1.225	32.685	0.470
Cu	-0.910	30.211	0.408
Co	-1.175	28.771	0.615
Zn	-0.845	69.022	0.493
Rb	-2.909	88.481	0.638

MIDDLE INTRUSIVE PHASES

ELEMENT	SLOPE	Y INTERCEPT	CORRELATION COEFFICIENT
SiO_2	0.808	54.498	0.874
Al_2O_3	-0.025	16.179	0.077
Fe_2O_3	-0.202	4.884	0.777
FeO	-0.108	3.116	0.697
CaO	-0.188	6.350	0.940
MgO	-0.150	3.763	0.959
Na_2O	0.011	5.046	0.070
K_2O	0.100	-0.481	0.554
TiO_2	-0.025	0.771	0.841
P_2O_5			
MnO	-0.003	0.090	0.187
H_2O	-0.047	1.523	0.595
Li	-1.131	56.747	0.190
Pb	5.192	-88.062	0.670
Ni	-1.664	42.614	0.424
Cu	-1.515	45.124	0.376
Co	-0.754	21.494	0.427
Zn	-3.849	122.803	0.913
Rb	0.355	38.842	0.052

LATE INTRUSIVE PHASES

ELEMENT	SLOPE	Y INTERCEPT	CORRELATION COEFFICIENT
SiO_2	0.949	51.023	0.900
Al_2O_3	-0.173	19.548	0.571
Fe_2O_3	-0.144	3.752	0.687
FeO	-0.124	3.452	0.828
CaO	-0.164	5.758	0.830
MgO	-0.154	3.892	0.934
Na_2O	-0.154	8.765	0.612
K_2O	0.107	-0.411	0.440
TiO_2	-0.022	0.694	0.997
P_2O_5	-0.022	0.564	0.870
MnO	-0.005	0.134	0.470
H_2O	-0.071	2.086	0.545
Li	1.040	10.478	0.248
Pb	-1.729	51.046	0.377
Ni	-1.108	31.644	0.256
Cu	-0.278	13.836	0.118
Co	-0.200	9.545	0.089
Zn	-2.790	104.907	0.796
Rb	2.752	-13.392	0.435

EARLY, MIDDLE AND LATE INTRUSIVE PHASES

ELEMENT	SLOPE	Y INTERCEPT	CORRELATION COEFFICIENT
SiO_2	0.747	55.616	0.854
Al_2O_3	-0.054	16.886	0.212
Fe_2O_3	-0.124	3.292	0.649
FeO	-0.149	3.988	0.850
CaO	-0.229	7.174	0.893
MgO	-0.063	2.322	0.207
Na_2O	-0.008	5.574	0.031
K_2O	0.119	-0.790	0.560
TiO_2	-0.026	0.780	0.917
P_2O_5	-0.014	0.388	0.828
MnO	-0.003	0.091	0.384
H_2O	-0.043	1.451	0.446
Li	-0.612	45.346	0.142
Pb	0.615	1.106	0.127
Ni	-1.184	32.996	0.340
Cu	-1.216	35.843	0.398
Co	-0.629	18.735	0.339
Zn	-1.047	69.268	0.762
Rb	1.036	22.511	0.183

FIGURE 2

GEOLOGY OF THE AULNEAU GRANITIC BATHOLITH, DISTRICT OF KENORA, ONTARIO, CANADA

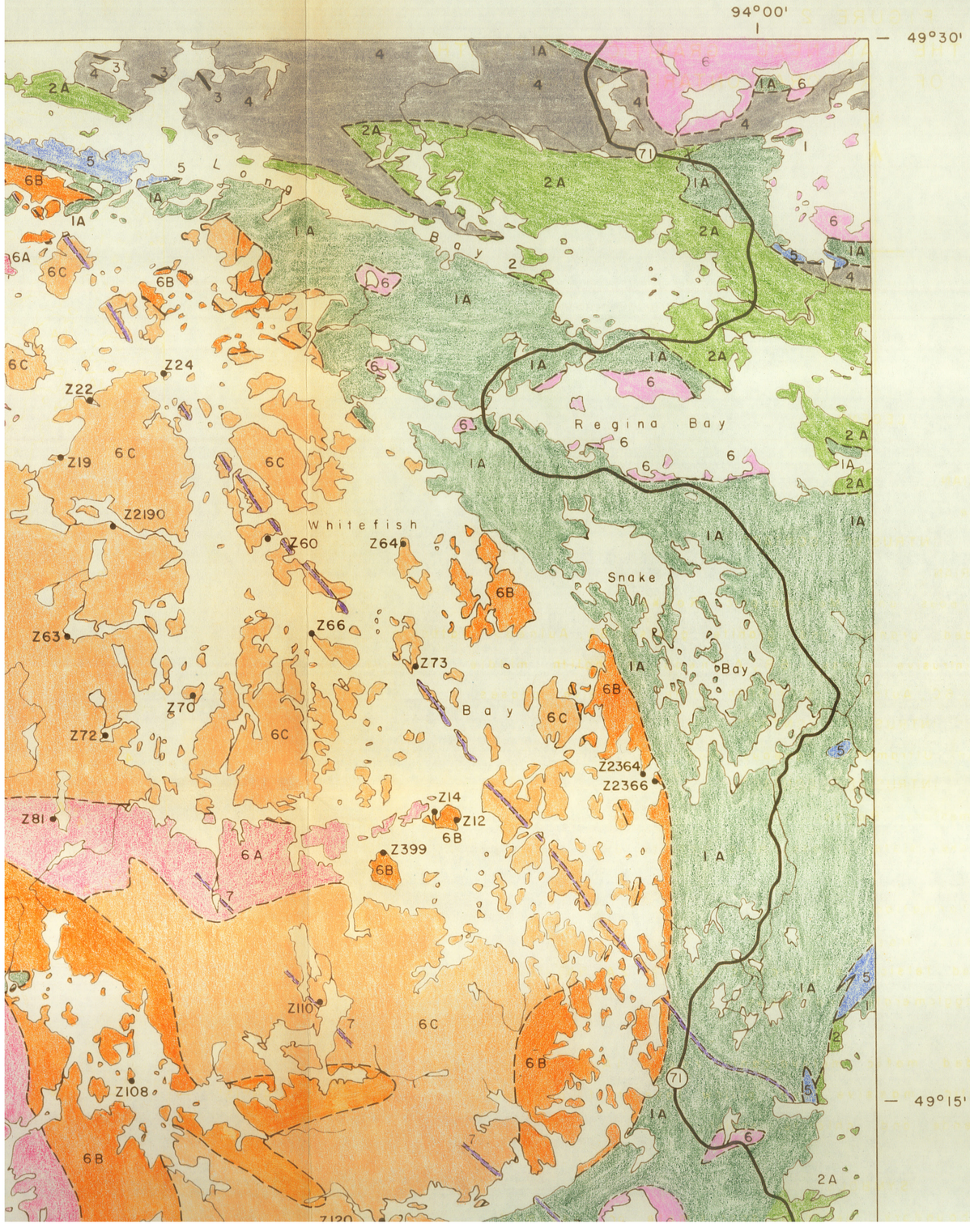

N

LEGEND

PRECAMBRIAN

LATE PRECAMBRIAN

7 — Diabase

INTRUSIVE CONTACT

EARLY PRECAMBRIAN

6 — Felsic Igneous and Metamorphic Rocks

Undivided granite and granite gneiss. 6A, Aulneau Batholith early intrusive phases; 6B, Aulneau Batholith middle intrusive phases; 6C, Aulneau Batholith late intrusive phases.

INTRUSIVE CONTACT

5 — Mafic and Ultramafic Igneous Rocks

INTRUSIVE CONTACT

Metasedimentary Rocks

4 — Greywacke, slate, arkose, mica schists and gneisses

3 — Iron formation

Metavolcanic Rocks

2 — Undivided felsic metavolcanic rocks. 2A, Rhyolitic and dacitic tuff, agglomerate and flows.

1 — Undivided mafic metavolcanic rocks. 1A, Basaltic and andesitic massive lava, pillow lava, tuff, agglomerate, hornblende and chlorite schist.

SYMBOLS

Geologic boundary, defined, approximate or assumed.

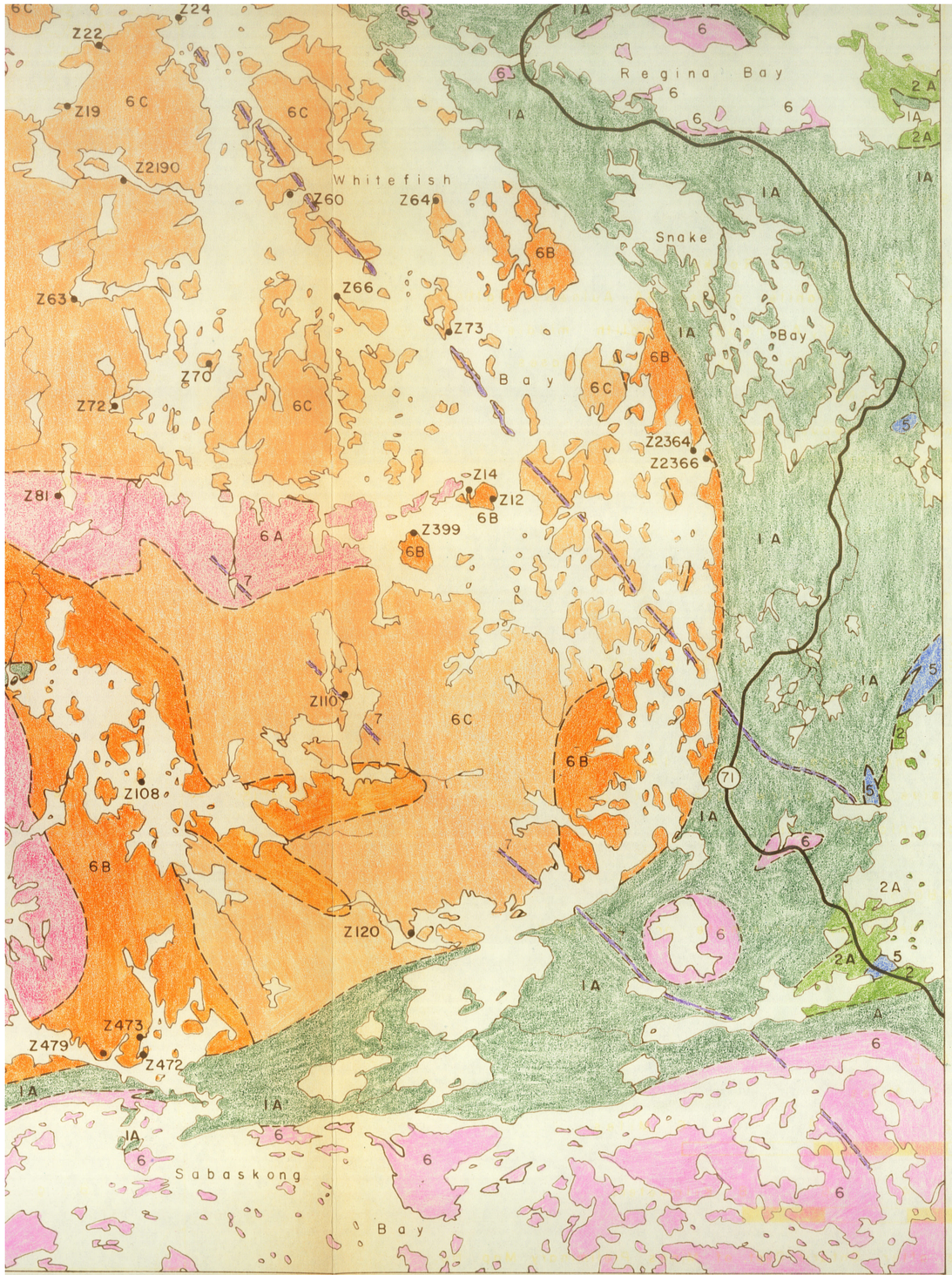

LEGEND

PRECAMBRIAN

LATE PRECAMBRIAN

7 — Diabase

INTRUSIVE CONTACT

EARLY PRECAMBRIAN

6 — Felsic Igneous and Metamorphic Rocks

Undivided granite and granite gneiss. 6A, Aulneau Batholith early intrusive phases; 6B, Aulneau Batholith middle intrusive phases; 6C, Aulneau Batholith late intrusive phases.

INTRUSIVE CONTACT

5 — Mafic and Ultramafic Igneous Rocks

INTRUSIVE CONTACT

Metasedimentary Rocks

4 — Greywacke, slate, arkose, mica schists and gneisses

3 — Iron formation

Metavolcanic Rocks

2 — Undivided felsic metavolcanic rocks. 2A, Rhyolitic and dacitic tuff, agglomerate and flows.

1 — Undivided mafic metavolcanic rocks. IA, Basaltic and andesitic massive lava, pillow lava, tuff, agglomerate, hornblende and chlorite schist.

SYMBOLS

Geologic boundary, defined, approximate or assumed.

•Z — Sample location.

SCALE

1 Inch to 2 Miles

2 0 2 4 6 Miles

2 0 2 4 6 8 Kilometers

Geological compilation by M.E. Chute after Ontario Dept. of Mines Preliminary Map No. P. 281 and unpublished maps by D.V. Ziehlke.

94°30'

49°30'

49°15'

Falcon Island

Lake of the Woods

Long Bay

Whitefish Bay

Miles Bay

Z51 Z90 Z91 Z89 Z94 Z86 Z98 Z100 Z85 Z194 Z97 Z104 Z145 Z150 Z22 Z24 Z19 Z15 Z2190 Z13 Z9 Z88 Z96 Z63 Z66 Z60 Z64 Z73 Z70 Z72 Z2364 Z2236 Z14 Z12 Z399 Z81 Z83 Z116 Z110 Z108 Z120

Falcon Island

Lake of the Woods

Big Island

Painted Rock Island

Miles Bay

Sabaskong Bay

Whitefish Bay

Z94 Z86 Z98 Z100 Z85 Z194 Z297 Z116 Z88 Z96 Z83 Z150 Z22 Z19 Z15 Z13 Z9 Z63 Z64 Z60 Z66 Z73 Z70 Z72 Z81 Z14 Z12 Z399 Z110 Z108 Z120 Z112 Z473 Z479 Z472

49°15'

94°30'